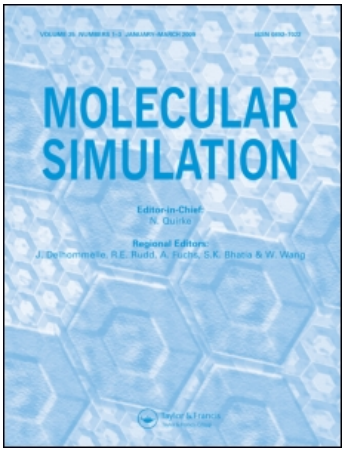

Molecular Simulation
Publication details, including instructions for authors and subscription information:
http://www.informaworld.com/smpp/title~content=t713644482

Experimental and computational studies of ZnS nanostructures

Said Hamad[a]; Scott M. Woodley[b]; C. Richard[b]; A. Catlow[b]
[a] Instituto de Ciencia de Materiales de Sevilla, CSIC-Universidad de Sevilla, Seville, Spain [b] Department of Chemistry, Computational Materials Chemistry, University College London, London, UK

To cite this Article Hamad, Said , Woodley, Scott M. , Richard, C. and Catlow, A.(2009) 'Experimental and computational studies of ZnS nanostructures', Molecular Simulation, 35: 12, 1015 — 1032
To link to this Article: DOI: 10.1080/08927020903015346
URL: http://dx.doi.org/10.1080/08927020903015346

Molecular Simulation
Vol. 35, Nos. 12–13, October–November 2009, 1015–1032

Taylor & Francis
Taylor & Francis Group

Experimental and computational studies of ZnS nanostructures

Said Hamad[a]*, Scott M. Woodley[b] and C. Richard A. Catlow[b]

[a]*Instituto de Ciencia de Materiales de Sevilla, CSIC-Universidad de Sevilla, Calle Américo Vespucio, 49, 41092 Seville, Spain;*
[b]*Department of Chemistry, Computational Materials Chemistry, University College London, Kathleen Lonsdale Building, Gower Street, London, UK*

(*Received 21 January 2009; final version received 22 April 2009*)

We review the experimental and computational studies of nanoparticulate ZnS, a system that has received much attention recently. We describe in detail how the nanoparticle structures evolve with increasing size. The results of the computational studies reveal intriguing families of structures based on spheroids, which have the greater stability for clusters with less than 50 ZnS pairs. More complex structures are predicted for larger systems, such as double bubbles, BCT nanoparticles and nanotubes.

Keywords: ZnS; nanoparticles; clusters; nanotubes; global minimisation

1. Introduction

The rapid growth of nanotechnology during the last decade has spawned an increasing interest in the search of methods to control the properties of nanoscale materials. Quantum size effects become large in materials with sizes in the range of the nanometre, which makes the properties of these materials dependent to a great extent on their size and structure [1,2]. It is therefore of key importance to understand the kinetic and thermodynamic factors that determine the size and structure of nanoparticles. Since the study of kinetic processes is complex, there have been great efforts directed towards the study of the thermodynamic factors that control the arrangement of the atoms or molecules that form the nanoparticles. The basic idea behind these efforts is the assumption that the nanoparticle will adopt the structure that minimises its energy. When dealing with crystals in the macroscopic scale, it is possible to obtain the morphology of a given crystal by employing the Wulff construction [3], which yields the equilibrium shape of a crystal knowing the energies of the surfaces that might appear in the crystal. This approach is not appropriate for nanoparticles; but we can still assume that the most likely structure that a given nanoparticle will adopt is that which minimises its energy. Thus, global minimisation techniques have been used to predict the structure of nanoparticles. In this article, we review the use of computational techniques in the study of an important semiconductor compound, ZnS, paying particular attention to the global optimisation techniques that provide information about the most stable nanostructures.

2. Experimental studies on ZnS nanostructures

ZnS belongs to the family of II–VI semiconductor compounds, which have a large number of applications in nanotechnology, as it is relatively easy to tailor the optical and electronic properties of the materials by controlling the shape of the nanostructures [4]. The shape of II–VI nanoparticles may be controlled by several methods: one is by manipulating the growth kinetics, injecting precursor molecules into a hot surfactant, which yields either monodispersive, nearly spherical quantum dots (QDs) or nanorods with different aspect ratios [5]. This ability to produce QDs routinely with controlled sizes and optical properties has found many applications in biological imaging [6]–[9], and their photosensitising properties are being investigated for their potential applications in cancer treatments [10,11], where UV irradiation might be absorbed by QDs and transferred selectively to cancer cells. The materials are also being studied for their potential uses in new electronic devices: a single CdSe QD can be optically excited in close proximity to a silver nanowire (NW) [12], which induces the QD to emit radiation coupled directly to guided plasmons in the NW, causing the wire's end to light up.

ZnS, which is among the most studied II–VI compounds, is a wide band-gap (3.7 eV) semiconductor and is one of the most important materials in optoelectronic applications, due to its good photoluminescent [13] properties; it is also used as a photocatalyst [14]. It can readily adopt two crystal structures [15], namely sphalerite (cubic or zinc blende phase) and wurtzite (hexagonal phase). Sphalerite is the most stable

*Corresponding author. Email: said.hamad@icmse.csic.es

ISSN 0892-7022 print/ISSN 1029-0435 online

DOI: 10.1080/08927020903015346
http://www.informaworld.com

form at room temperature, while the less dense wurtzite is stable above 1020°C at atmospheric pressure and is metastable (as a macroscopic phase) under ambient conditions. Of course, the stability of the two phases is influenced by the morphology of the material: thermodynamic analysis, which makes use of surface energy data, shows that smaller wurtzite nanoparticles are more thermodynamically stable than sphalerite [16]. For particles as small as 7 nm, the temperature for the transformation from sphalerite to wurtzite is only 25°C. The origin of the change in the order of stability of the two crystal structures is the free energy γA (the product of the surface free energy and the surface area). For macrocrystalline phases, this term is negligible and the stability is determined by the difference in energy between the two phases. But for nanostructures, the surface to bulk ratio is large enough to make the term significant. In this case, the difference between the surface energies of the two phases plays a key role. Changing the surface energies therefore induces changes in the crystallinity of the nanoparticles [16]. This change in surface energies might be achieved, for example, by changing the solvent in which the particles are immersed. When 3 nm ZnS nanoparticles synthesised in methanol are dried out, they adopt a very disordered structure. But when water is adsorbed on the surface, they undergo a reversible water-driven structural transformation [17] to the sphalerite phase, as shown in Figure 1.

Using the appropriate synthesis conditions, it is possible to tune the morphology of ZnS structures in order to create nanobelts [18] (Figure 2(a)) with the wurtzite polymorph, which is the more desirable polymorph for its optical properties. Due to their high aspect ratio, ultrafine ZnS nanobelts [19] are being extensively studied as field emitters and are highly useful in novel nanoscale electric and optoelectronic devices [20]. Other exotic structures such as nanosheets [21] (Figure 2(b)) and nanoflowers [22] (Figure 2(c)), which show optical properties that can be finely tuned, might also be obtained by solution synthesis routes. Low-cost thermal evaporation routes yield ZnS multiangular branched nanostructures [23] with needle-shaped tips (Figure 2(d)), which show good optical properties with potential application in the fabrication of displays. Self-aggregation/assembly methods are very valuable tools for building materials with desired nanostructures. Their use allows the creation of two coexisting levels of nanostructural order, by synthesising monodispersive (2.8 nm) ZnS nanoparticles in a one-step

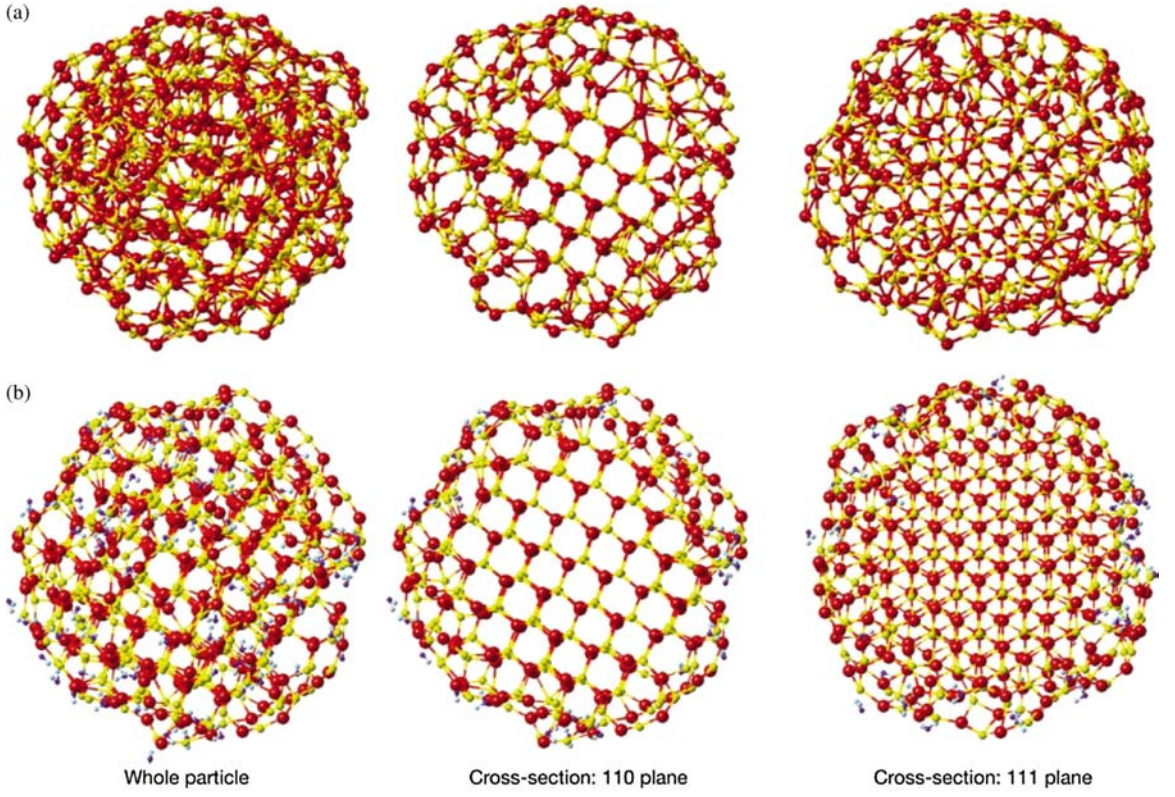

Figure 1. Molecular dynamics (MD) predictions of the structure of a 3 nm ZnS nanoparticle. (a) Without surface-bound water, and (b) with surface-bound water. S atoms yellow, Zn red, O blue, H light blue. Central cross sections through the particles give a clearer picture of internal structure. Regular interior (1 1 0) and (1 1 1) planes are evident in both structures, but in the absence of water ligands, the outer shell is severely distorted. Reprinted from [17] by permission of Macmillan Publishers Ltd; © 2003.

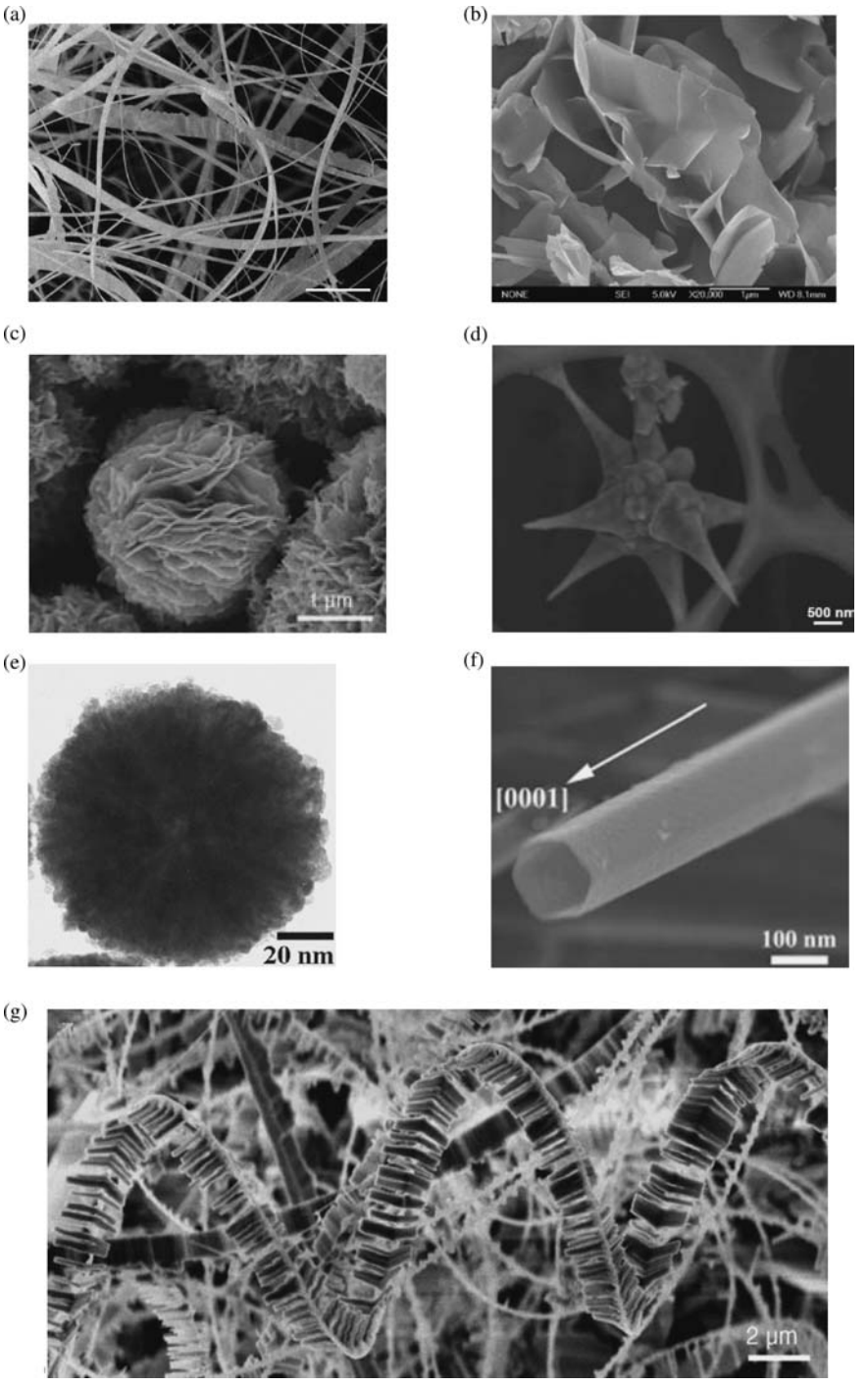

Figure 2. SEM and TEM images of various ZnS nanostructures. (a) ZnS nanobelts with wurtzite structure. (b) Aggregate of ZnS nanosheets, formed by treating ZnS nanoparticles at 230°C in 17 M NaOH. (c) Wurtzite ZnS flowers composed of nanosheets. (d) Multiangular branched ZnS nanostructure with needle-shaped tips. (e) A single nanosphere, indicating self-assembly of ZnS nanoparticles. (f) Single ZnS nanotubes, clearly showing hexagonal cross sections. (g) Branched ZnS nanohelix. The Y-shaped branches always point towards the inside of the coil, regardless of the handedness of the nanohelix. (a) Reprinted from [18] by permission of Macmillan Publishers Ltd; ©2005. (b) Reprinted from [21] by permission of the American Chemical Society; ©2006. (c) Reprinted from [22] by permission of Wiley-VCH Verlag GmbH & Co. KGaA; ©2005. (d) Reprinted from [23] by permission of the American Chemical Society;©2008. (e) Reprinted from [24] by permission of Elsevier; ©2007. (f) Reprinted from [25] by permission of Wiley-VCH Verlag GmbH & Co. KGaA; ©2005. (g) Reprinted from [26] by permission of Wiley-VCH Verlag GmbH & Co. KGaA; ©2006.

colloidal precipitation method [24], which spontaneously aggregate and self-assemble to form dense nanospheres of 100–120 nm sizes with optimal optical properties (Figure 2(e)). Since temperature influences strongly the rates of nucleation, growth and diffusion, it plays a crucial role in self-assembly methods, as shown by Yin et al. [25] who found that high temperatures (1500°C) were needed to form single-crystalline ZnS nanotubes with hexagonal cross sections (Figure 2(f)). The use of lower temperatures resulted in the formation of solid NWs. In some cases, it is possible to form complex structures with ordered features that range from the nanoscale to the microscale. Vapour deposition processes can be tuned to form hierarchical structures, in which ZnS helices several micrometres long are formed by two structures: a spine with helical shape [26], from which a secondary structure of Y-shaped branches (all with the same size) grows towards the axis of the helix, rotating as they follow the geometry of the helix (Figure 2(g)). The existence of hierarchical order in nanostructures often leads to the emergence of unexpected properties, such as the ability to withstand ultra-high stress and strain as shown by hierarchically hollow CdS nanoparticles [27].

Determining the atomic structure of nanomaterials is essential to understanding the processes that take place during their use in nanotechnological applications and much effort is being devoted to that goal. Structure determination of nanocrystals by X-ray diffraction is inherently difficult as they often show an appreciable degree of disorder [28]. Two methods that are commonly used to elucidate the structure of nanomaterials are transmission electron microscopy (TEM) and extended X-ray absorption fine structure (EXAFS). Neither, however, provides enough information to determine uniquely the structure of the materials. As Urban stated in a recent review [29] of TEM studies of nanomaterials: 'understanding the results is generally not straightforward and only possible with extensive quantum-mechanical computer calculations'. This combination of computer modelling and experiment is the basis of what has been named 'complex modelling'. Billinge and Levin [30] suggested 'complex modelling' as a powerful method to solve the structure of nanomaterials, employing experimental and modelling techniques in a self-consistent computational framework [30]. Similar techniques have been successfully applied to solve crystalline structures with very complex unit cells, such as those of metal-organic frameworks [31]–[33]. In the study of clusters with only a small number of atoms or molecules, the use of experimental techniques has been very limited so far, and computational techniques are the main source of information about their structures and properties. In the next section, we will focus on the studies carried out on ZnS clusters, with particular emphasis on the different computational techniques that have been employed.

3. Computational studies on ZnS nanostructures

3.1 Early theoretical studies

In 1989, Lippens and Lannoo [34] reported one of the first theoretical studies of ZnS nanoparticles (although, at that time, they were referred to as crystallites instead of nanoparticles). They employed tight binding approximations to calculate the band gap of small CdS and ZnS crystals with sizes between 1 and 6 nm (20–25,000 atoms). The calculations strongly overestimated the band gaps, although they provided a correct description of the size effect of small semiconductor crystallites. Employing cluster processes, another line of research investigated chemisorption processes on ZnS surfaces. In 1992, Muilu and coworkers [35] carried out Hartree–Fock calculations of the adsorption of $ZnCl_2$ and $Zn(CH_3)_2$ on the polar (1 1 1) zinc-blende surface of ZnS and ZnSe, in which the surfaces were modelled as single- and double-layer $(ZnS)_n$ clusters, with $n = 3–15$. These simplistic models provided information about the preferential sites for adsorption. Later on, they used the translational symmetry of two-electron integrals to make possible the study of larger ($n = 3–240$) clusters [36], obtaining a linear dependence of the cohesive energy on the surface to bulk ratio. The study of nanoparticles was too demanding for the computational resources available at that time. But the discovery of carbon fullerenes [37] and hollow metallo-carbohedrenes [38,39] prompted extensive calculations on clusters, which were much smaller and therefore more easily tractable with *ab initio* techniques. For example, Smalley and co-workers used density functional theory (DFT) calculations to study hollow cage structures of M_8X_{12} [40] (M = Ca, Ti, Zn, Sc and Al, X = B, C and N). All the atoms are three-coordinated with each cluster composed of 12 pentagons, which are joined to form a dodecahedron with T_h symmetry. In 1994, Behrman et al. [41] carried out one of the first studies of II–VI compounds clusters. Employing Born–Mayer interatomic potentials, they performed molecular dynamics (MD) simulations of $(ZnO)_{15}$, with the initial structure being a fragment of the most stable bulk phase at ambient conditions for ZnO (the hexagonal, wurtzite structure). During the simulation, one of the bonds connecting each of the four coordinated atoms is broken so that after 10 ns the cluster becomes a spheroid in which all the atoms are three-coordinated, formed by the arrangement of four- and six-atom rings. The $(ZnO)_{12}$ cluster was also studied, and it was suggested that it might be a magic cluster, due to its particularly symmetric structure [41]. A recent review of computational studies of ZnO clusters can be found in reference [42]. After this MD study, the existence of fullerene-like clusters has been predicted and observed experimentally for many materials, such as ZnS [43], ZnO [44–47], group IIa–VIa clusters [48], AgI [49], BN [50,51], B [52], FeC [53], GaP [54], AlN [55] or other group III–V [56,57] clusters.

3.2 Nanoparticles capped with organic ligands

Another relevant field of solid-state science, in which the study of small clusters was of key importance, was the study of II–VI QDs capped with organic ligands. In 1993, Herron et al. [58] synthesised a single crystal in which the building unit (Figure 3) was a $Cd_{32}S_{14}$ cluster capped with organic molecules, namely $Cd_{32}S_{14}(SC_6H_5)_3$-DMF_4. Xie [59] synthesised $Zn_8S_{15}N_2$ clusters capped with ligands, and was able to form crystals (Figure 3). These materials have been useful to understanding the dependence on cluster size of properties such as the band gap, since the periodicity of the crystals allows the knowledge of the exact geometry of the clusters [60], which can then be directly related to the properties studied. Bertoncello et al. [61] studied ligand-capped ZnS_4, Zn_4S_{10}, $Zn_{10}S_{16}$ and $Zn_{10}S_{20}$ clusters, by coupling DFT to UV electronic and X-ray photoelectron spectroscopy. They found that the only cluster that reasonably mimics both the structural arrangement and the electronic structure of the bulk ZnS sphalerite phase is $Zn_{10}S_{16}$. We have already noted the big influence that even small quantities of adsorbed water molecules have on relatively large (>3 nm) ZnS nanoparticles, causing them to change their crystallinity order [62–64]. It is therefore obvious that the presence of capping organic molecules in small (typically smaller than 2 nm) nanoparticles will be one of the main factors involved in the growth and the stability of these small bulk-like nanoparticles [65], and that the growth processes that govern their formation are likely to be different from those of non-capped nanoparticles. The physical properties of these capped nanoparticles are also affected by the presence of the ligands, as recently shown for capped Zn_8S_{15} nanoparticles [59]. Tight binding DFT calculations show that even passivation with small ligands (—H and —OH) has an important effect on the electronic and optical properties of ZnSe nanoparticles [66]. MD simulations of the self-assembly of capped CdTe nanoparticles [67] have provided an atomistic view of the template-free, spontaneous self-organisation of the nanoparticles to form free-floating particulate sheets, in a process reminiscent of those happening in biological systems.

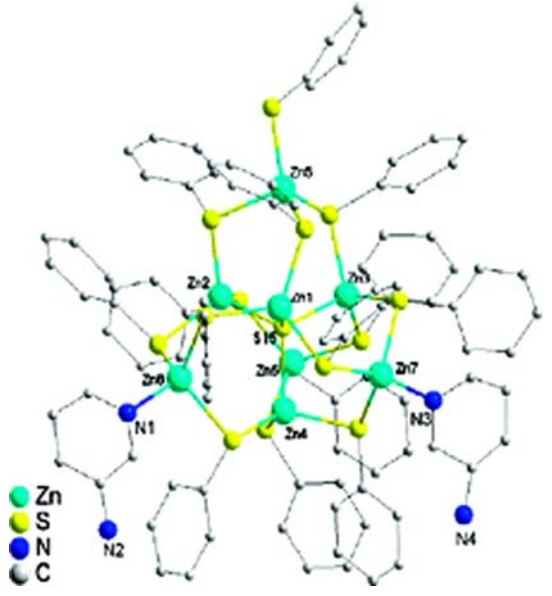

Figure 3. $Zn_8S_{15}N_2$ cluster structure, including the C atoms of the ligands. H atoms are not shown for clarity reasons. Reprinted from [59] by permission of the American Chemical Society; © 2008.

3.3 Aqueous ZnS clusters

Metal–sulphide (including ZnS) nanoparticles are present in aquatic sulphidic systems, where they can control the mobility and bioavailability of pollutants such as zinc, mercury and silver [68]. They also act as intermediates of mineralisation reactions [69]. The initial stages of nucleation and growth of ZnS nanoparticles in aqueous solutions has therefore been a subject of extensive experimental research [70–75], but theoretical studies are very scarce. One of the main centres of attention has been the study of the predominant Zn complexes in water. UV–vis and titration experiments [71] show that initially neutral clusters (stoichiometry 1 Zn: 1 S) are formed, and when additional sulphide is added, the stoichiometry changes to 2 Zn: 3 S. Gel electrophoresis suggests that these clusters are negatively charged. The clusters might be interpreted to be $Zn_4S_6(H_2O)_4^{4-}$ clusters. The experiments did not provide information about the structure of these clusters, although Luther et al. [71] carried out classical molecular mechanics calculations of the condensation of two hydrated $Zn_3S_3(H_2O)_6$ rings to form one $Zn_4S_6(H_2O)_4^{4-}$ cluster, and observed that the latter cluster could have the structure of a fragment of sphalerite. But no other cluster structures were studied, so there is no comparison between the stability of the sphalerite-like clusters and any other non-bulk-like cluster. The existence of the structural units of the crystal is not a pre-requisite for the formation of the corresponding crystal. For example, the metastable α-polymorph of glycine molecular crystals is readily obtained by crystallization from water solution, instead of the most stable γ-polymorph. This fact has often been attributed to the presence of glycine dimers [76] (characteristic of the α-polymorph) in water solution, a simplistic view that has been recently refuted [77,78].

Tiemann et al. [74] employed *in situ* stopped flow UV absorption spectroscopy to study the first stages of the nucleation and growth of ZnS in aqueous solution. They found that the growth of the clusters in solution is very fast. The clusters initially formed are negatively charged even in neutral pH conditions. During the first 60 ms, there is a substantial decrease in particle concentration [75],

indicating that there is a high degree of particle coalescence. The size of the smaller particles observed in these experiments [74,75] (at 1.8 ms) is between 7 and 8 Å. MD simulations provide an atomistic picture of formation of ZnS clusters from Zn^{2+} and S^{2-} ions in water solution [79]. The clusters are negatively charged, since they tend to have more S than Zn atoms (Figure 4(a)). There might be a thermodynamic driving force for this effect, as Zn^{2+} ions form very stable hexa-aquo complexes ($Zn^{2+}(H_2O)_6$), while S^{2-} ions do not interact strongly with water. The formation of a Zn—S bond is a very exothermic event, and therefore the bonds in the clusters are not easily broken, which is in accordance with the experimentally observed preference of coalescence over Ostwald ripening [75] and with previous EXAFS studies [80]. Figure 4(b) shows a schematic of growth found for two separate clusters in a 1.25 M solution of ZnS. The clusters are initially planar, formed by four- and six-atom rings, but as they grow they become more spherical. The largest cluster formed after 6 ns of simulation, $(Zn_9S_{11})^{4-}$, is shown in Figure 4(c). It is an open bubble-like structure, which has no water molecules

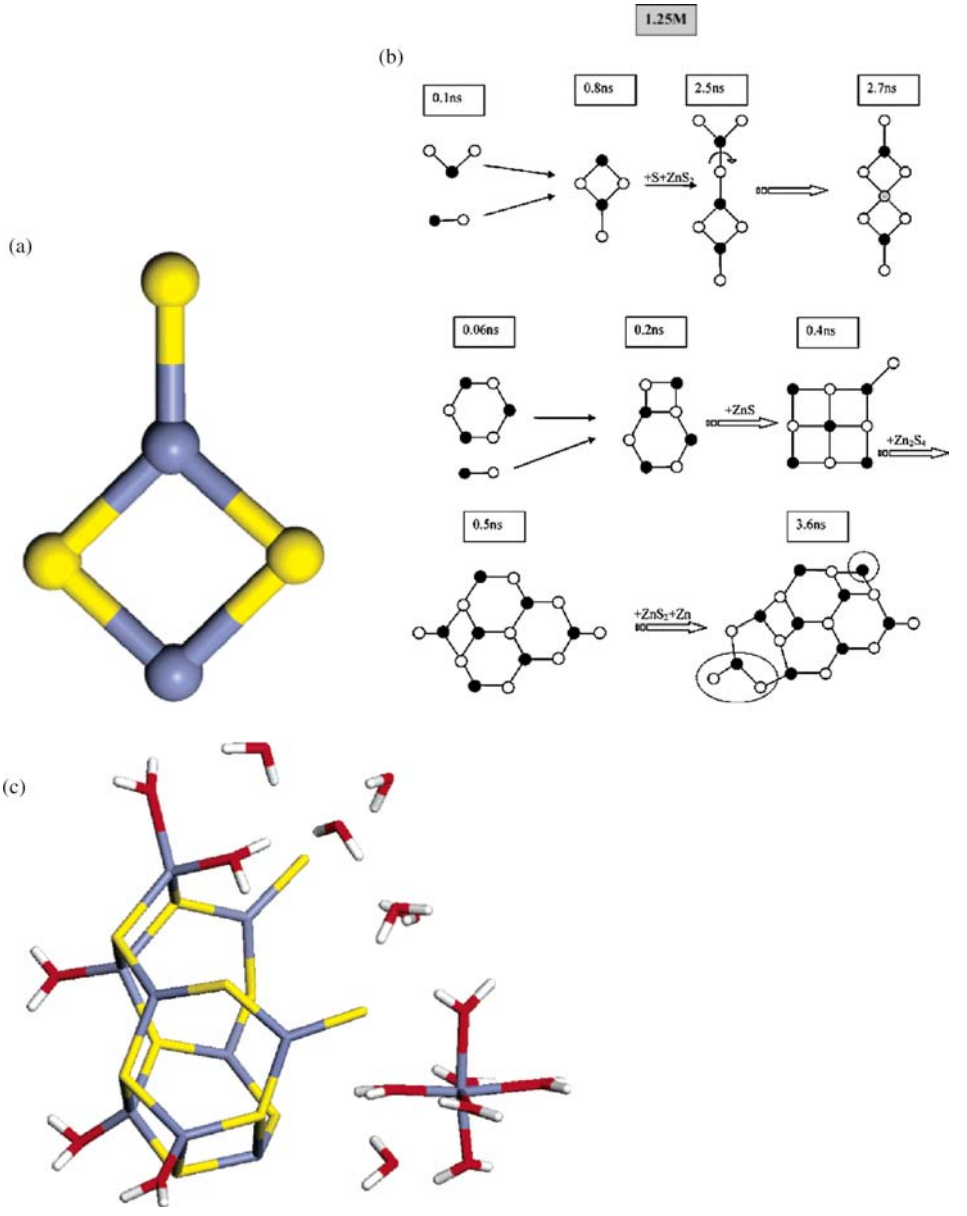

Figure 4. (a) Structure of the $(Zn_2S_3)^{2-}$ cluster formed in classical MD simulations of ZnS cluster growth. (b) Schematic view of the growth sequence of a 1.25 M ZnS solution at room temperature. (c) $(Zn_9S_{11})^{4-}$ cluster formed after 6 ns simulation in the system with 1.25 M concentration. The structure is non-planar, due to the presence of three squares. There are no water molecules bound to the internal side of the developing cluster, suggesting that the addition of more atoms would easily form a closed cluster without water inside. Reprinted from [79] by permission of the American Chemical Society; © 2005.

inside. The simulations therefore suggest that, after the formation of planar clusters, closed bubble-like clusters with no water molecules inside will be formed.

Although successful for very small clusters, this growth model however does not account for larger nanoparticles which have bulk-like structures. Zhang et al. [81] performed MD simulations of water adsorption processes of ZnS nanoparticles (3 and 5 nm), coupled with temperature-programmed desorption experiments. The results from both techniques show that each surface Zn atom can adsorb 2.5 water molecules, while each S atom can adsorb 0.5 water molecules [81]. Their simulations showed that water–water interactions are not as strong on the curved surfaces of the nanoparticles as on the flat surfaces of bulk crystals, which provided a theoretical reason why more water molecules can be adsorbed by ZnS nanoparticles (and with higher binding energy) than by bulk ZnS surfaces.

Huang et al. [82] carried out a study of the adsorption of water, ammonia and other Lewis base molecules on ZnS clusters, employing BLYP/DNP calculations. Although the molecules induce a certain amount of structural rearrangement, there is no rupture of Zn—S bonds, and all molecules are chemisorbed. Their results suggest that the stronger the basic nature of the adsorbed molecule, the stronger the interaction with the ZnS clusters. This effect might be used to stabilise small ZnS clusters and nanoparticles, reducing particle aggregation.

Chemical vapour deposition (CVD) is one of the techniques employed in the fabrication of electronic devices. Sarifi and Achenie [83] investigated the clusters formed in the initial stages of growth in CVD processes by means of B3LYP/6−311+$G(d,p)$ calculations. They considered different structures of clusters with one Zn, one S and two H atoms to study the initial, transition and final states of the reaction $Zn + HSH \rightarrow ZnS + H_2$. Despite the small size of the model system, they found very good agreement between their enthalpy and free energy of reaction data and those obtained from experiments. This method could be used to study the formation of other ZnS clusters (including water molecules), which would provide very valuable information on the kinetics of ZnS cluster growth.

3.4 Small ZnS clusters

Matxain et al. [84] made one of the first attempts to obtain the most stable structures of ZnS clusters. They did not employ global minimisation techniques but made use of chemical intuition to create a set of stable $(ZnS)_n$ clusters ($n = 1–9$). The clusters were optimised within the DFT framework, using the hybrid three-parameter B3LYP functional [85], and the effective core potentials (ECP) and shared-exponent basis sets of Stevens et al. [86] (SKBJ) to model the core electrons. They found that there are two competing factors involved in the stabilisation of $(ZnS)_n$ clusters: (i) in the most stable configuration, the S—Zn—S angles are as close as possible to 180°; and (ii) stabilisation of the system is enhanced by higher coordination. As a result, the global minima for the smaller clusters ($n = 1–5$) are planar, ring structures, whereas for $n = 6–9$ the most stable clusters are three-dimensional spheroidal structures. Once the structure of the most stable clusters was found, they studied electron excitation energies for the three smallest clusters [87], employing three different methods: configuration interaction singles (CIS), time-dependent density-functional theory (TDDFT) and multi-reference configurational interaction (MR-CI). The latter method was used as reference with which to compare the results obtained with the other two methods, due to the lack of experimental data. They found that both CIS and TDDFT methods need to include several polarisation functions in the basis sets in order to yield correct electron excitation energies. The less computationally demanding calculations that yielded results comparable to those of MR-CI calculations are TDDFT calculations employing the MPW1PW1 functionals [88] and the ECP–SKBJ basis sets mentioned above, augmented with 1 sp, 2 d and 2 f functions. This type of calculations was later employed [90] to study larger $(ZnS)_n$ clusters ($n = 1–9$). The electronic excitations occur typically from non-bonding p orbitals of S atoms, which are perpendicular to the molecular plane in the smaller, ring-like clusters and normal to the spheroid surfaces for the larger clusters [89]. The electronic excitation energies of the spheroid clusters lie within the visible range of the spectrum. They also found that a reasonably good approximation to the electronic excitation energies of the largest clusters could be obtained by calculating the difference between the B3LYP Kohn–Sham energies of the orbitals. The energies obtained with this method [90] are within 10% of those calculated employing TDDFT.

One consequence of the hollow structure characteristic of these clusters is the possibility of enclosing different atoms, which could induce changes in their physical properties, as happens in the case of fullerene clusters. No experimental studies on this subject have been published so far, although DFT techniques have been used to study the properties of small ZnS and ZnO clusters [90,91] doped with Mn, Li, Na, K, Cl and Br.

The clusters discussed so far are stoichiometric (i.e. they have the same number of Zn and S atoms). Chuchev and Belbruno [92] carried out an investigation on small, non-stoichiometric Zn_nS_m and $Zn_nS_m^+$ clusters ($1 \leq n, m \leq 4$), using B3LYP/CEP-121G calculations. Their results provide an energetic basis for the observed excess sulphur clusters in mass spectrometric experiments. There is a large energy penalty for the formation of clusters with short Zn—Zn distances, although it is energetically

feasible to produce clusters with S—S bonds [92]. The removal of an electron affects the cluster geometries, causing, in some cases, rather large atomic rearrangements. This ability to form S—S bonds might also be a reason why small ZnS clusters in water solution tend to be sulphur rich [74].

3.5 *Magic clusters*

The first study of $(ZnS)_n$ clusters with $n > 9$ was carried out in 2002 by Burnin and Belbruno [93]. They employed a laser beam to ablate ZnS and ZnO surfaces. The positive ions produced were analysed with a time-of-flight (TOF) mass spectrometer. The most remarkable finding is the existence of a prominent peak with a mass of 1280 amu (in the case of ZnS), suggesting that $(ZnS)_{13}^+$ is a magic number cluster. Another prominent peak is found at approximately 3315 amu, which corresponds to a $(ZnS)_{34}^+$ cluster. For ZnO, there were no 'magic' clusters. In order to understand the formation of the $(ZnS)_{13}^+$ magic cluster, they employed semi-empirical MNDO calculations to scan a number of different structures of $(ZnS)_{13}^+$ clusters. The MNDO structures were then optimised at the HF/CEP-31G level, and the energies were calculated with single-point calculations at the B3LYP/CEP-31G level. They studied four different $(ZnS)_{13}^+$ cluster structures: I (basket-like), II (open cage), III (zinc-blende) and IV (wurtzite) structures. Structures I and II were formed by the arrangement of four-, six- and eight-member rings, where all atoms are three-coordinated, as predicted previously for some MgO clusters [94] using genetic algorithms. Structures III and IV initially had some four-coordinated atoms, although upon minimisation they became open structures with only three-coordinated atoms. The most stable configurations were clusters I and II. These results suggest that ZnS clusters might be more stable in spheroidal structures, in accordance with the results of Matxain et al. [84] for smaller clusters.

Kasuya et al. [95] carried out a study similar to that of Burnin and Belbruno [93] (laser ablation followed by TOF mass spectrometry and a subsequent computational study), although in addition to ZnS they also studied CdSe, CdS and ZnSe. $(CdSe)_{13}^+$, $(CdSe)_{33}^+$ and $(CdSe)_{34}^+$ were found to be magic clusters, as in the case of ZnS [93]. The main difference between the two studies is that Kasuya et al. [95] suggested a different structure to account for the high stability of the $(CdSe)_{13}^+$ cluster, the so-called core-cage cluster, in which 12 Se and 13 Cd atoms form a cage with 3 four-member and 10 six-member rings, which encloses a Se atom in the centre of the cluster, as shown in Figure 5. Employing DFT calculations, they showed that the binding energy of the $(CdSe)_{34}$ cluster is higher than that of $(CdSe)_{33}$ and $(CdSe)_{35}$ clusters (by 0.005 and 0.04 eV per CdSe unit, respectively), but unfortunately they did not provide similar data for $(CdSe)_{13}$. More recently, Woodley et al. [96] carried out an extensive study of the stability of $(MX)_{13}$ clusters for a range of II–VI compounds (ZnO, CdO, ZnS, CdS, ZnSe, CdSe, ZnTe and CdTe) using a DFT (PBE/DNP) approach and structures found by means of genetic algorithm search of the interatomic potential-based energy landscape for ZnS. They advanced the hypothesis that magic numbers may be related to the number of different configurations accessible within thermal range from the global minimum. The $(ZnS)_{13}$ core-cage cluster, where one Zn atom is contained within the pore of a bubble, was among the less stable of a series of different structures, while the most stable structure investigated was a spheroidal cluster with only three-coordinated atoms and no atoms inside – thus

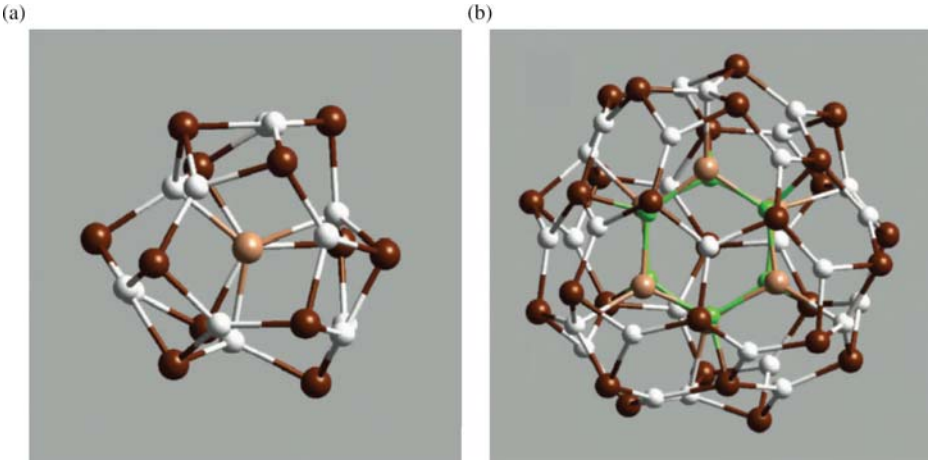

Figure 5. Structures of the $(CdSe)_n$ core-cage nanoparticles calculated to be most stable, viewed down a threefold symmetry axis. (a) $(CdSe)_{13}$ has 3 four-membered and 10 six-membered rings on the cage of 12 Se (dark brown) and 13 Cd (white) ions with a Se (light brown) ion inside. (b) $(CdSe)_{34}$ has a truncated-octahedral morphology formed by a $(CdSe)_{28}$-cage (Se, dark brown; Cd, white) with 6 four-membered and 8 × 3 six-membered rings. A $(CdSe)_6$ cluster (Se, light brown; Cd, green) encapsulated inside this cage provides additional network and stability. Reprinted from [95] by permission of Macmillan Publishers Ltd; © 2004.

corroborating and extending the initial findings of Burnin and Belbruno [93]. Both groups have performed further studies in order to shed some light onto this controversy. The balance of interatomic interactions in the series of 1–1 compounds is the focus of current work by Woodley and co-workers. In turn, Burnin et al. [97] has carried out a further study on the structure and stability of $(ZnS)_n$ and $(ZnS)_n^+$ clusters for $n = 1$–16. They employed algorithms that generate a large number of possible structures having predefined constraints. These clusters were then optimised at the B3LYP/6−311+G* level of theory. The smaller clusters ($n < 6$) have planar structures for neutral and positive clusters. Large neutral clusters have the geometries of close-cage polyhedra (with only three-coordinated atoms) formed by four- and six-member rings. The structures of large positive clusters are similar to that of the neutral clusters, but with an important difference: there are 2 two-coordinated atoms (one S and one Zn atom) in each cluster. Only for $n = 12$, 15 and 16, do the structures of the neutral and positive clusters coincide [97], being the close-cage polyhedra with only three-coordinated atoms. The core-cage structure of the $(ZnS)_{13}$ cluster suggested by Kasuya et al. [95] was not considered in that study. However, this structure was considered in another experimental and computational study of ZnSe, CdSe, ZnS and CdS clusters [98]. It was found that the core-cage structure was the global minimum energy structure for $(CdS)_{13}$ and $(CdSe)_{13}$ clusters, but it was only a local minimum for $(ZnS)_{13}$ and $(ZnSe)_{13}$ clusters. Therefore, they suggest that Cd has a higher tendency than Zn to stabilise structures with four-coordinated atoms. Although a partial understanding of the TOF spectra was obtained [98] with the analysis of the cluster energies calculated with DFT, the controversy over the reasons why magic clusters appear in II–VI materials is far from over, and our investigations show that different basis sets and exchange and correlation functionals can lead to differing results, which will be reported in the near future.

3.6 Larger ZnS clusters

The structures of small $(ZnS)_n$ clusters ($n < 10$) can be obtained with reasonable confidence using chemical intuition to create small sets of possible structures. But the number of possible configurations increases exponentially as the number of atoms increases, making essential the use of global optimisation techniques that generate low-energy structures. A recent review of the use of different global minimisation techniques (genetic algorithms, Monte Carlo basin hopping, simulated annealing (SA), etc.) to study a wide range of systems can be found in reference [99]. Spano et al. [100] employed SA simulations based on suitable interatomic potentials [101] to obtain the most stable structures of $(ZnS)_n$ clusters with $n = 1$–47. The clusters with global energy minimum were hollow, cage-like structures, formed by the polyhedral arrangement of four-, six- and eight-member rings, in which all the atoms are three-coordinated. They denoted these as bubble clusters [100]. They have also been called spheroids [84] or Euler clusters [98] by other authors. Some representative bubble clusters are shown in Figure 6. One of their main features is that they follow Euler's theorem of closed polyhedra, which means that the number of four-, six- and eight-member rings in a $(ZnS)_n$ cluster is related by the following two formulae:

$$N_{6-\text{ring}} = n - 4 - 2N_{8-\text{ring}},$$

$$N_{4-\text{ring}} = 6 + N_{8-\text{ring}}.$$

For perfect bubbles (all atoms at the surface and three-coordinated), there is a minimum of '$n - 4$' six-member rings and 6 four-member rings, when there are no eight- or larger member rings. For every eight-member ring created, there is a loss of 2 six-member rings and an increase in 1 four-member ring. It can be argued that bubble ZnS clusters are more stable when composed of six-member rings (hexagonal faces): an increase in either four- or eight-member rings tends to destabilise the structures, and typically the most stable structures do not have any eight-member rings (or additional four-member rings by increasing the average coordination number). Moreover, the four-member rings (tetragons) tend to be separated from each other (an additional hexagonal ring can be formed from two adjacent tetragons by breaking just one bond). An analogous observation can be made with five-member rings in fullerenes, which is another system in which Euler's theorem applies. In fullerenes, the isolated pentagon rule [102] favours structures in which pentagons (the analogous of our squares) are isolated. In bubble clusters, the building units are squares, hexagons and octagons, and the rule could be named as the isolated tetragon rule [97]. For small clusters, the existence of non-bulk-like clusters was generally accepted, but for clusters as large as $(ZnS)_{47}$ it was thought that the system was large enough to create at least a small bulk-like region in the centre, so the hollow bubble clusters provided by the SA process were unexpected. In order to test whether the bubble clusters appeared as a result of inaccuracies in the interatomic potentials employed [101], a series of DFT calculations (PW91 functional with effective core potential and double numerical plus polarisation basis sets) were carried out, which yielded more accurate energies of bubble clusters and other bulk-like clusters [100]. The DFT calculations showed that the higher stability of bubble clusters with respect to the bulk-like clusters was not due to a failure of the interatomic potentials, since the average difference in energy between the two structural families was ~200 kJ/mol.

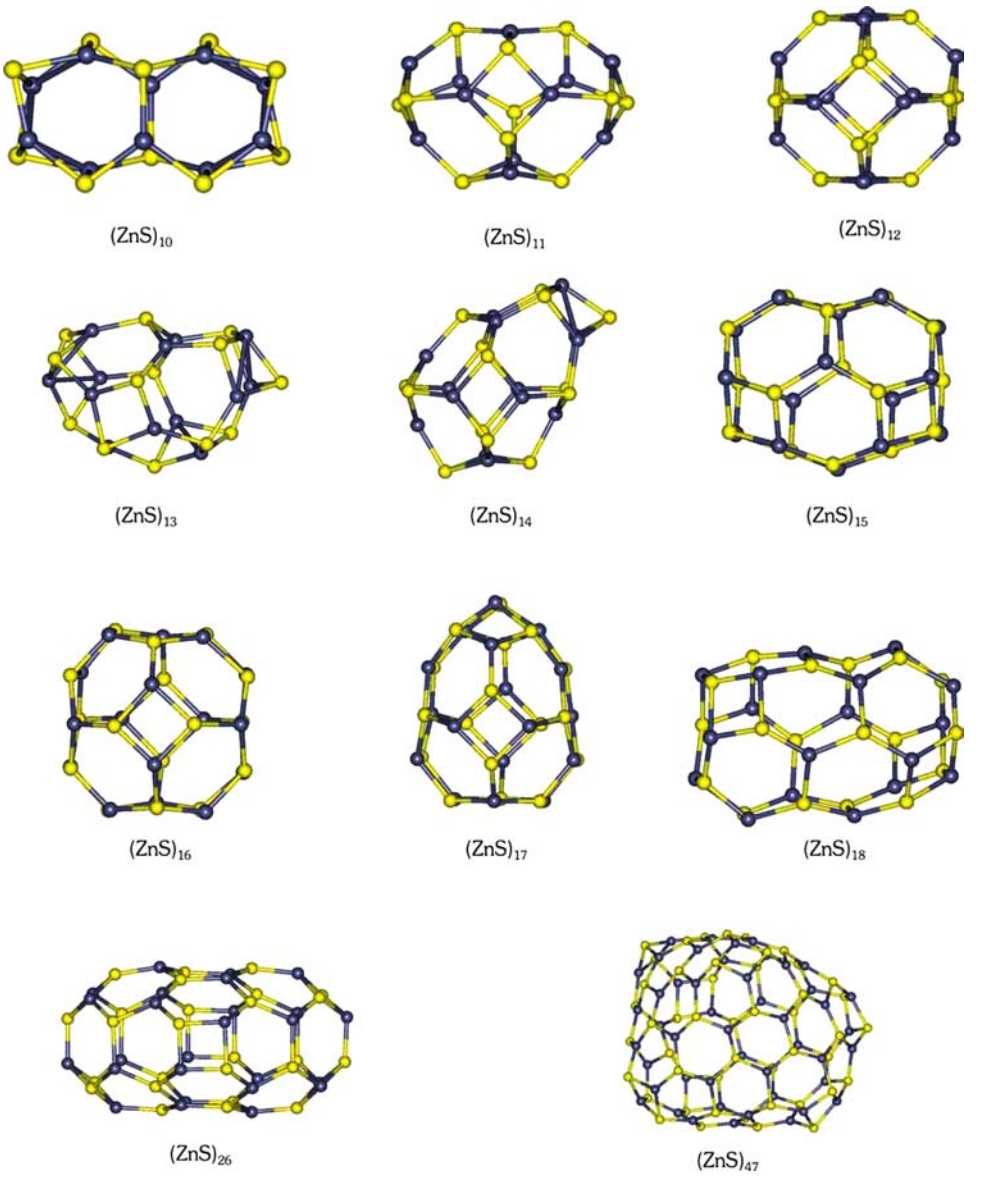

Figure 6. Predicted structures of selected bubble clusters. Blue sticks refer to sulphur and yellow to zinc. Reprinted from [43] by permission of the American Chemical Society; © 2005.

TDDFT calculations show [103] that the clusters with higher oscillator strengths are $(ZnS)_{18}$, $(ZnS)_{20}$ and $(ZnS)_{26}$. Their excitation energies are of the order of 4.9eV. There are several experimental measures of the band gaps of ZnS nanoparticles. Calandra et al. [104] measured the band gap to be in the range of 5.25–6.0 eV for nanoparticles between 2 and 6 nm. The band gap of 2 nm ZnS sphalerite nanoparticles has also been measured [105] as 4.5 eV. For hollow 2.8 nm ZnS nanoparticles, the band gap was 4.3 eV. The band gaps (calculated as the HOMO–LUMO energy difference) of $(ZnS)_n$ clusters [43] with $n = 10$–47 lie within the range 4.4–4.8 eV. For clusters [43] with bulk-like structures, the band gaps were in the range 3.65–3.95 eV. The wide range of structures that the nanoparticles adopt and the experimental difficulties in elucidating them can explain the disparity in the reported values for the band gap.

It is observed experimentally that for sufficiently large sizes (>3 nm) ZnS nanoparticles adopt bulk-like (sphalerite or wurtzite) structures, in which most of the atoms are four-coordinated, so there is a size at which bubble clusters become less stable than other cluster geometries. In order to study the sizes at which this transition in stability takes place, another set of SA simulations were carried out [43,106] for $(ZnS)_n$ clusters with sizes $n = 50$, 60, 70 and 80. The results were again surprising, as the most stable structures turned out

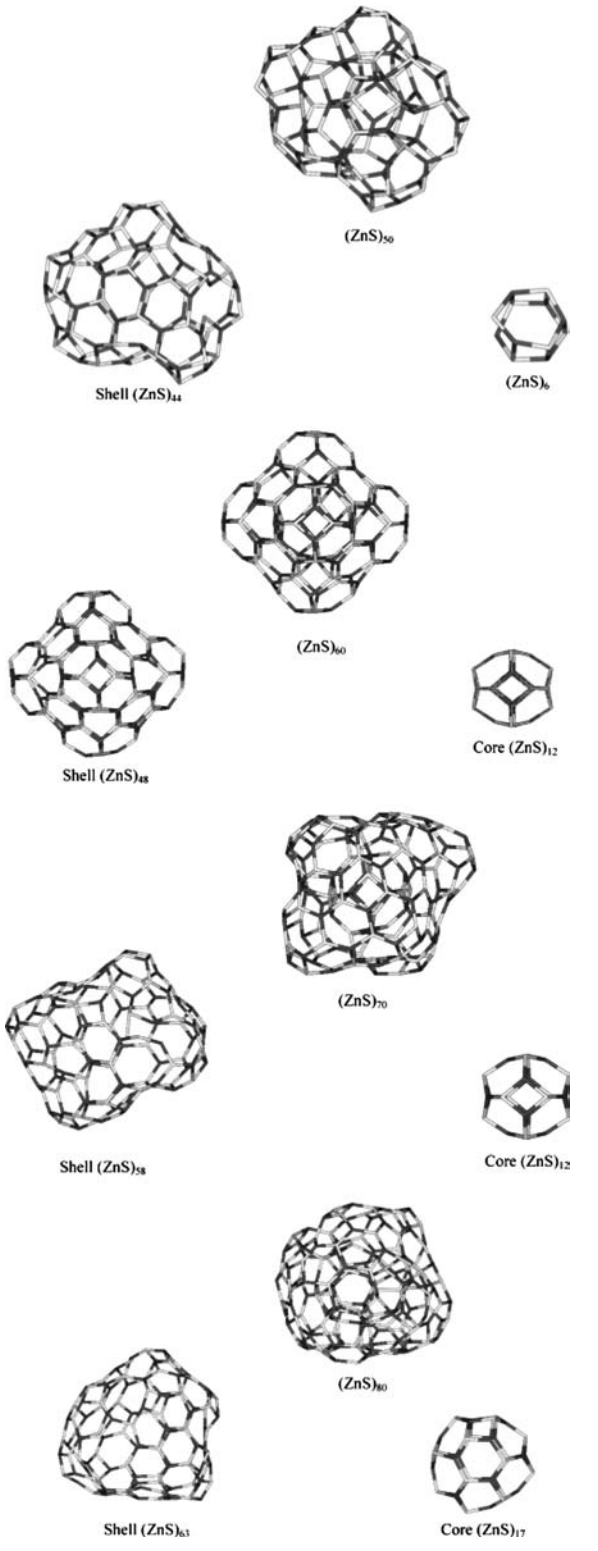

Figure 7. Structures of the four bubble clusters studied. The complete structures are shown in the centre of each panel, while the innermost and outermost clusters are shown below them. Light grey sticks refer to sulphur and dark grey to zinc. Reprinted from [43] by permission of the American Chemical Society; © 2005.

to be core-shell structures in which one bubble cluster was enclosed inside a larger cluster. These new clusters were denoted double bubbles. Figure 7 shows the double bubbles ($n = 50$, 60, 70 and 80) as well as the component single-bubble clusters. The core bubble in the case of $n = 50$ is the $(ZnS)_6$ cluster. $(ZnS)_{12}$ is the core bubble in the two intermediate sizes ($n = 50, 60$), while in the largest ($n = 80$) double bubble, the cluster enclosed is the $(ZnS)_{17}$ bubble. In order to test the validity of the predictions based on interatomic potentials, the difference in energy between a double-bubble $(ZnS)_{60}$ cluster and two $(ZnS)_{60}$ bulk-like clusters was calculated [107] with both interatomic potentials and DFT calculations (PW91/ecp-dnp). The energy differences were around 12 eV for both methods. For the $(ZnS)_{70}$ cluster, the energy difference was 6.65 and 3.85 eV when calculated with DFT and interatomic potential methods, respectively. The two methods therefore agree in the prediction of double bubbles as the most stable structures for $(ZnS)_n$ clusters with $n = 50$, 60, 70 and 80.

Sarkar and co-workers have carried out a series of theoretical studies regarding the stability of the different $(ZnS)_n$ cluster structures. In their earlier work, they reported [108] that tight binding DFT calculations predict small ($n < 17$) bubble clusters to be more stable than bulk-like (zinc-blende) clusters, which agrees with the PW91/ecp-dnp results obtained by Hamad et al. [43] and Spano et al. [106] mentioned above. But they also reported that for larger clusters, especially $(ZnS)_{58}$ and $(ZnS)_{68}$, bulk-like clusters are more stable than bubble clusters. However, in a more recent investigation [109], where they compared a different set of stable hollow, bubble clusters with zinc-blende and wurtzite $(ZnS)_n$ clusters for $n = 10$, 16, 37, 57, 68, 86 and 116, their reported DFT–tight binding results showed that hollow clusters are more stable than bulk-like clusters [109]. An interesting result of that study is the existence of a minimum in the plot of the band gap versus number of atoms in the cluster, for both single- and double-bubble clusters. The minimum is located between $n = 80$ and 110, and it is attributed to the balance between two competing effects: quantum size effects (which cause a decrease in band gap as the cluster size increases) and curvature-induced $\sigma-\pi$ hybridisation (which causes an increase in band gap as the cluster size increases).

As mentioned above, energetic considerations are obviously very important, but kinetic effects may also have great influence in the outcome of ZnS crystallisation. Very few studies have considered the growth dynamics of large bubble and bulk-like clusters. The discovery of hollow, multi-shelled Co_xS_y nanoparticles [110] led Pal et al. [111] to carry out a theoretical study of the influence of diffusion rates on the dynamics of ZnS cluster growth, starting from different building units (namely ZnS, Zn_2S_2, Zn_5S_5 and Zn_8S_8). Although hollow clusters are more stable, under certain conditions, the energy barriers to their

formation are larger than that for bulk-like clusters [111], which can be used experimentally to exert some kinetic control and favour one particular structure over the other.

3.7 Transition from three-coordinated to four-coordinated clusters: BCT structure

Global minimisation techniques predict structures of $(ZnS)_n$ clusters (for $n = 10–80$), which are predominantly made up of arrangements of three-coordinated atoms. Even in double bubbles, where a network of four-coordinated atoms connect the two bubbles [106], most of the atoms are still three-coordinated. In order to obtain the structure of larger clusters, in which four-coordinated atoms are predominant, Hamad and Catlow [107] performed a SA study of two large $(ZnS)_n$ clusters: $n = 256$ and 512. The clusters cut from the zinc-blende structure were simulated with MD at 3000 K. The high temperature caused the clusters to melt, losing all crystalline order. The temperature was slowly decreased, until in one part of the melted nanoparticles a crystalline nucleus appeared, which expanded throughout the whole nanoparticle. Nucleation events are very rare, and very long simulations on high performance terascale computers were needed. Figure 8 shows the structure of the two nanoparticles after crystallisation has taken place. The interior of the nanoparticles is crystalline, while there is some degree of disorder in the outer shell, which is also observed in other MD studies of nanoparticles [62], as shown in Figure 1. But the unexpected feature of the two $(ZnS)_{256}$ and $(ZnS)_{512}$ nanoparticles is the structure of the crystalline interior. At first sight, they resemble the hexagonal phase of ZnS (wurtzite), but closer examination shows that the unit cell contains four- and six-member rings (Figure 9), as in the case of bubble clusters. The structure is topologically equivalent to that of the BCT zeolite, so this new ZnS phase was denoted the BCT phase. The two nanoparticles with the BCT structure were obtained just by decreasing the temperature in MD simulations; no template or capping agents were needed. This is an indication of the absence of large energy barriers, which suggests that there might be a simple kinetic route for the experimental synthesis of these clusters. The existence of BCT structures is not limited to ZnS. Morgan and Madden [112–114] and Morgan [115] have found domains with the BCT structure in modelling nanocrystal systems such as ZnO and CdSe. Doll et al. [116,117] observed the formation of metastable crystalline BCT structures in BN [116] and LiF [117] from *ab initio* SA simulations. BCT structures have also been observed

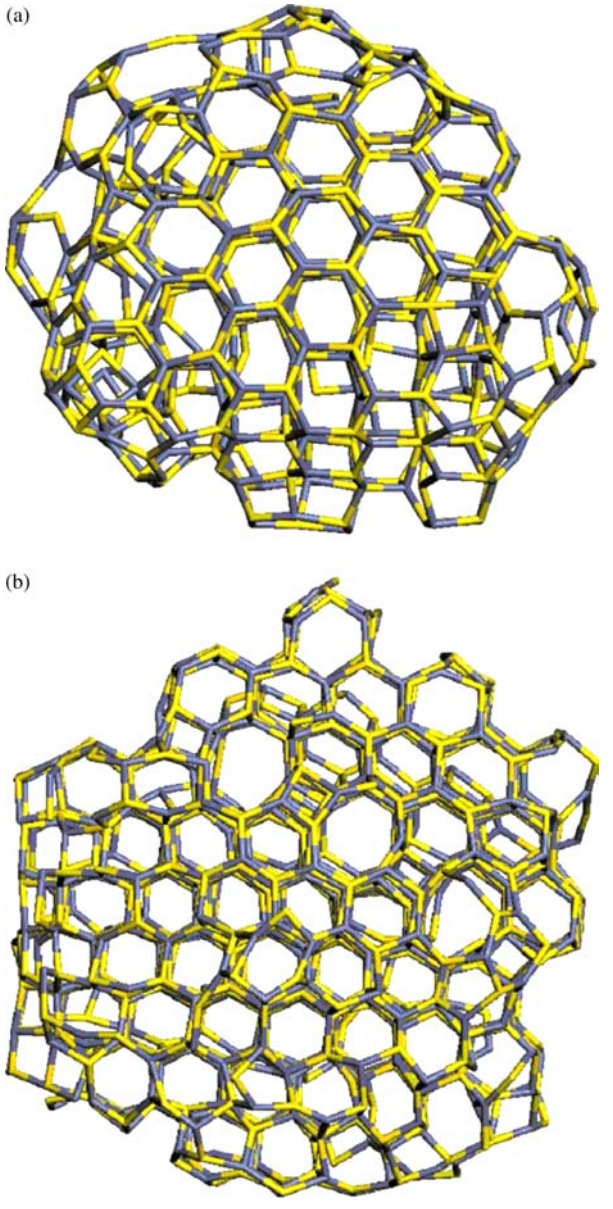

Figure 8. Structures of two clusters, obtained with SA. (a) $(ZnS)_{256}$ and (b) $(ZnS)_{512}$. Light grey sticks refer to sulphur and dark grey to zinc. Reprinted from [107] by permission of Elsevier; © 2006.

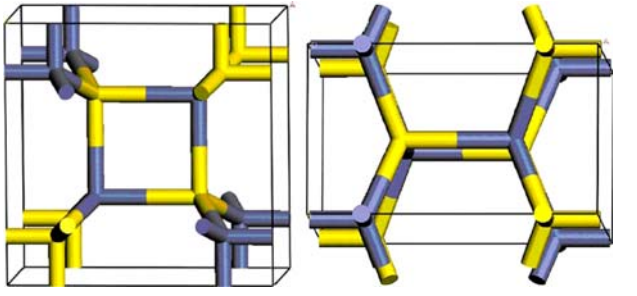

Figure 9. Front and top views of the unit cell that generates the $(ZnS)_{256}$ and $(ZnS)_{512}$ clusters, which is the same structure as the BCT zeolite, although in zeolites each Zn and S site is occupied by Si atoms, with O atoms connecting them, creating a more open structure. Reprinted from [107] by permission of Elsevier; © 2006.

experimentally in PbSe nanoparticles [118]. Sayle et al. [119] observed the formation of BCT structures in MgO and CaO nanoparticles. And in an MD study of the formation of mesoporous materials via self-assembly of amorphous ZnO and ZnS nanoparticles, Sayle et al. [119,120] also observed the formation of extended regions with both wurtzite and BCT structures. The emergence of these two structures and the transformation from one to another during the process of crystallisation of the mesoporous material is shown in Figure 10. As shown in Figure 10(e), there is a very smooth transition from the two structures, and therefore there is no need to create defects to release structural strain.

In order to check whether the nanoparticles crystallised with the BCT structure for kinetic reasons rather than for thermodynamic reasons, the energies of large sets of clusters with different structures were calculated [107] using DFT and interatomic potentials. Figure 11(a) shows the energies, calculated with interatomic potentials of $(ZnS)_n$ clusters ($n = 18–80$) with four different structures: (a) cubic, (b) hexagonal, (c) BCT and (d) the bubble clusters obtained from SA simulations. Clusters with cubic, hexagonal and BCT structures are generated without dangling bonds and with the lowest dipoles possible, in order to minimise the distortions after optimisation. It is clear that that bubble clusters are the most stable in all cases, followed by the BCT clusters. The energies of six hexagonal and BCT clusters (in the range $n = 18–70$) were also calculated with the PW91/ecp-dnp level of theory, obtaining very good agreement with the results derived from interatomic potentials [107], which enhances our confidence in the validity of the results. Figure 11(b) shows the same data as Figure 11(a), extending the range of the clusters from $n = 18$ to 560, which corresponds to sizes between 1 and 4 nm. For clusters larger than $(ZnS)_{80}$, the most stable clusters have the BCT structure. It is worth noting that two interatomic potentials for ZnS were employed in that

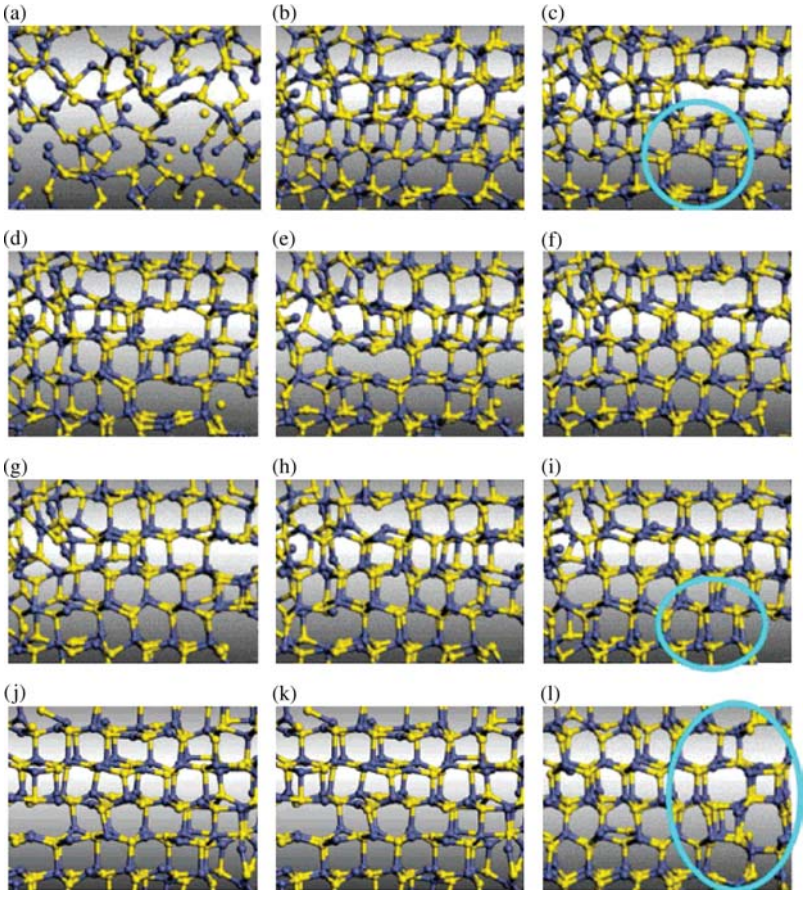

Figure 10. Snapshots taken during the MD simulation of the 2D system showing the crystallisation of the ZnS; ball-and-stick model representations of the Zn (blue) and S (yellow) atom positions. (a) After 5 ps showing the amorphous/molten ZnS; (b) after 500 ps revealing the (partial) crystallisation of the ZnS; (c) after 700 ps, the area circled accommodates a four- to eight-membered ring structure; (d) 750 ps; (e) 800 ps; (f) 850 ps; (g) 900 ps; (h) 950 ps; (i) 1000 ps is the region highlighted by the blue circle has now rearranged into a wurtzite structure; (j) 1250 ps; (k) 1500 ps; (l) 1895 ps the region highlighted has returned to a four- to eight-membered ring conformation. Reprinted from [120] by permission of the American Chemical Society; © 2006.

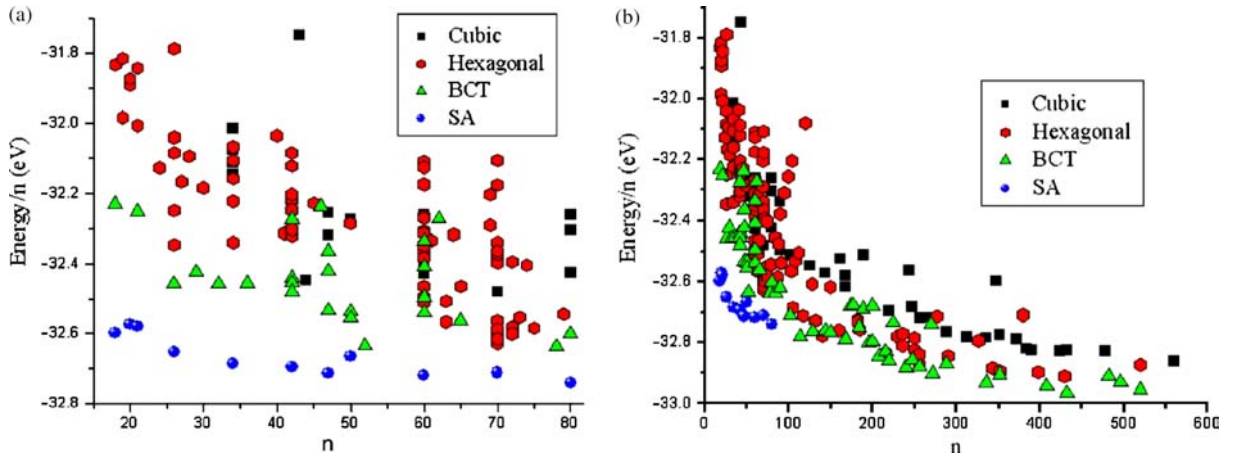

Figure 11. (a) Energies of $(ZnS)_n$ clusters for $n = 18-80$, after the geometry optimisation has been performed using interatomic potential energy minimisation techniques. The structure of the clusters is indicated in the legend. The SA clusters are bubble and double bubbles, which were obtained from SA methods. (b) Energies of all the geometry optimised $(ZnS)_n$ clusters for $n = 18-560$, using IPEM techniques. The structure of the clusters is indicated in the legend. Reprinted from [107] by permission of Elsevier; © 2006.

study, those obtained by Hamad and Catlow [107] and those obtained by Wright and Gale [121]. The latter did not perform as well as the former in predicting the structure and energies of clusters, since it was fitted in order to model accurately the two phases of ZnS [121], while the comparison with some data from DFT calculations of ZnS clusters was taken into account during the fitting of the former potential [107].

DFT calculations (PW91/ecp-dnp) show that a ZnS solid with BCT structure is 69.1 kJ/mol less stable than the cubic (sphalerite) phase, suggesting that there must be other specific energetic factors inducing the small nanoparticles to adopt that crystallise phase, rather than the cubic or hexagonal phases that are the most stable crystalline phases for larger nanoparticles and bulk solids. The greater stability of the BCT-based cluster structures probably arises from the ability to accommodate distortions within these structures more easily than that in the bulk-like structures. Cubic and hexagonal clusters undergo considerable rearrangements upon minimisation, because their crystallinity makes it very difficult to achieve a structure with low dipole and no dangling bonds. On the other hand, bubble clusters have very small dipoles, and their surface strain is very low. Since BCT clusters present four- and six-member rings naturally in their bulk interior, and there is a smooth transition between the bulk and the surface of the nanoparticles, which makes them very stable.

ZnS nanoparticles with a BCT structure have not yet been observed experimentally, which might be due to three main reasons: (a) this structural motif is not as stable as simulations would predict or the most stable clusters are not BCT structures. However, we note that the BCT structures have been predicted independently using either MD or global minimisation techniques for several systems and using a range of measures of stability, (b) they have not been synthesised for kinetic reasons or (c) they could have been synthesised, but characterised as either wurtzite or sphalerite because it has features similar to both of them [107] while the diffraction techniques become less reliable in the range of the particle size of interest. If kinetic issues were the cause, then the use of several crystallisation methods employing different solvents (similar to the polymorph screenings performed in pharmaceutical sciences) could help their synthesis, since the solvent has a strong influence on the nanoparticle crystallinity [61–63,122].

3.8 ZnS nanotubes and NWs

If hollow, polyhedral ZnS clusters, in which all the atoms are three-coordinated, can be considered as the ZnS-based structures analogous to C-based fullerenes, the analogy can be extended to another important type of C-based structures: nanotubes. This subject has attracted much experimental [25,123–127] and theoretical [128–131] attention recently. Pal et al. [128] carried out the first computational study of ZnS nanotubes, employing tight-binding DFT calculations. They found a certain degree of buckling in the structure, i.e. Zn atoms tend to be displaced towards the nanotube axis, while S atoms tend to be displaced in the opposite direction, which is similar to what happens in surfaces [101] and hollow clusters [108]. The buckling decreased from $\sim$0.4 to $\sim$0.19 Å as the nanotube radius increased from 4 to 9 Å. The band gap behaves differently depending on the way the graphite-like ZnS structure is folded to create the nanotubes. For zigzag nanotubes, $(n, 0)$, the band gap decreases as the radius of the nanotube increases, whereas for armchair nanotubes (n, n), there is a broad maximum in the band gap [128], between 6 and 8 Å. Pal et al. [132] have employed tight-binding DFT calculations in conjunction with genetic

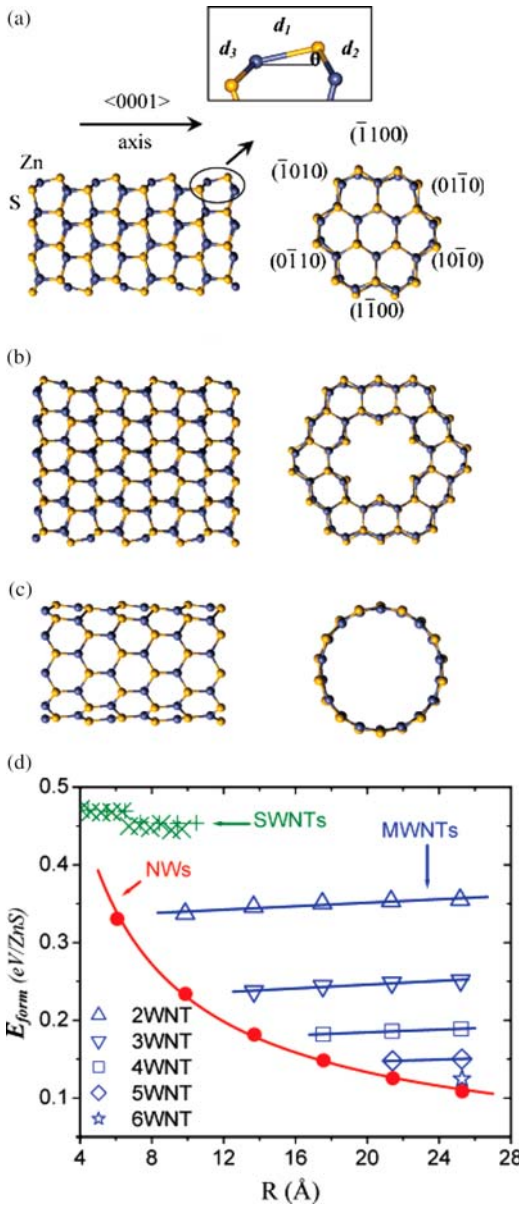

Figure 12. Side (left column) and top views (right column) of (a) ZnS NW; (b) faceted double-walled ZnS nanotube; (c) (9, 0) single-walled ZnS nanotube. The structural parameters (d_1, d_2, d_3, θ) representing the surface relaxations are indicated in the inset of Figure (a). (d) Evolution of the formation energy (E_{form}) of ZnS-NWs (red solid circles), multi-walled ZnS-NTs (open up triangles, down triangles, squares and diamonds), and ZnS-SWNTs (crosses) as a function of radius. The red solid line represents the fitting data of ZnS-NWs given by the expression $E_{\text{form}} = 0.689/R^{0.78}$. The radii of the multi-walled ZnS-NTs are the outer radii. Reprinted from [129] by permission of the American Chemical Society; © 2008.

algorithms to study systems with 10, 16, 37, 57 and 68 ZnS units. Contrary to other studies, they found that the most stable structures are ring-like configurations, with large radii and band widths of just two atoms. Most of the atoms in these structures are two-coordinated. Since these low-coordinated, low-density structures are totally unexpected, they compared their energies with those of hollow clusters, using DFT calculations with ecp-dnp, as implemented in the SIESTA code. Their results suggest that rings are more stable than hollow clusters by 0.4–0.8 eV/atom.

Li et al. [129] made use of interatomic potential-based [102] and PBE/DZP calculations to study ZnS nanotubes (NTs), nanovires (NWs) and nanosheets. Figure 12 shows an example of a NW (with wurtzite structure), single-walled nanotube (SWNT) and double-walled nanotube (DWNT). Both NWs and multi-walled NTs (MWNTs) are hexagonally faceted in order to minimise the energy. The formation energies of all the structures are shown in Figure 12(d). The most stable structures are NWs, followed by MWNTs, and the least stable structures are SWNTs, which do not undergo significant stabilisation as the size increases. All NWs and NTs are found to be wide band-gap semiconductors, with a direct band gap at the Γ point.

It is interesting to compare the relative stability of these structures with that of bubbles, calculated per formula unit. PBE/DNP calculations [131] show that the formation energy of DWNTs is lower than that of the $(ZnS)_{60}$ double bubble, which in turn is lower than those of SWNTs, $(ZnS)_{12}$ and $(ZnS)_{48}$ single bubbles. This complex landscape of possible structures is analogous to that of C-based structures, where several different structures (graphite layers, fullerenes, nanotubes, etc.) are observed. Ultimately the kinetic effects are the ones that determine the formation of the particular structures, and these structures can be stabilised by large energy barriers that stop the aggregation and transformation processes that would lead to the formation of the most stable diamond structure.

4. Summary

Nanoparticulate ZnS shows a fascinating range of structures, which contrast with those observed for the bulk material. Computer simulation methods have proved particularly effective in modelling and predicting possible structures, although further experimental work to test predictions would be of great interest. This is therefore a good example of a research field in which a close collaboration between computational and experimental work is needed.

Acknowledgements

We are grateful to the EU (funding through the NUCLEUS project) and EPSRC (Portfolio Grant EP/D504872). We also thank Eleonora Spanó and Alexey A. Sokol for useful discussions and contributions. S.H. would like to thank the Spanish Ministry of Science and Innovation for funding through a 'Juan de la Cierva' Fellowship.

References

[1] A.P. Alivisatos, *Semiconductor clusters, nanocrystals, and quantum dots*, Science 271 (1996), pp. 933–937.

[2] A.P. Alivisatos, *Perspectives on the physical chemistry of semiconductor nanocrystals*, J. Phys. Chem. 100 (1996), pp. 13226–13239.

[3] C. Rottman and M. Wortis, *Statistical-mechanics of equilibrium crystal shapes – interfacial phase-diagrams and phase-transitions*, Phys. Rep. Rev. Sect. Phys. Lett. 103 (1984), pp. 59–79.

[4] C. Burda, X. Chen, R. Narayanan, and M.A. El-Sayed, *Chemistry and properties of nanocrystals of different shapes*, Chem. Rev. 105 (2005), pp. 1025–1102.

[5] X. Peng, L. Manna, W. Yang, J. Wickham, E. Scher, A. Kadavanich, and A.P. Alivisatos, *Shape control of CdSe nanocrystals*, Nature 404 (2000), pp. 59–61.

[6] X. Gao, Y. Cui, R.M. Levenson, L.W.K. Chung, and S. Nie, In vivo *cancer targeting and imaging with semiconductor quantum dots*, Nat. Biotech. 22 (2004), pp. 969–976.

[7] M.N. Christof, *Nanoparticles, proteins, and nucleic acids: biotechnology meets materials science*, Angew. Chem., Int. Ed. 40 (2001), pp. 4128–4158.

[8] A. Fu, W. Gu, B. Boussert, K. Koski, D. Gerion, L. Manna, M. Le Gros, C.A. Larabell, and A.P. Alivisatos, *Semiconductor quantum rods as single molecule fluorescent biological labels*, Nano Lett. 7 (2007), pp. 179–182.

[9] N.L. Rosi and C.A. Mirkin, *Nanostructures in biodiagnostics*, Chem. Rev. 105 (2005), pp. 1547–1562.

[10] R. Bakalova, H. Ohba, Z. Zhelev, M. Ishikawa, and Y. Baba, *Quantum dots as photosensitizers?* Nat. Biotech. 22 (2004), pp. 1360–1361.

[11] A.C.S. Samia, X. Chen, and C. Burda, *Semiconductor quantum dots for photodynamic therapy*, J. Am. Chem. Soc. 125 (2003), pp. 15736–15737.

[12] A.V. Akimov, A. Mukherjee, C.L. Yu, D.E. Chang, A.S. Zibrov, P.R. Hemmer, H. Park, and M.D. Lukin, *Generation of single optical plasmons in metallic nanowires coupled to quantum dots*, Nature 450 (2007), pp. 402–406.

[13] C. Feldmann, T. Jüstel, C.R. Ronda, and P.J. Schmidt, *Inorganic luminescent materials: 100 years of research and application*, Adv. Funct. Mater. 13 (2003), pp. 511–516.

[14] Q. Zhao, Y. Xie, Z. Zhang, and X. Bai, *Size-selective synthesis of zinc sulfide hierarchical structures and their photocatalytic activity*, Cryst. Growth Des. 7 (2007), pp. 153–158.

[15] B. Gilbert, B.H. Frazer, H. Zhang, F. Huang, J.F. Banfield, D. Haskel, J.C. Lang, G. Srajer, and G.D. Stasio, *X-ray absorption spectroscopy of the cubic and hexagonal polytypes of zinc sulfide*, Phys. Rev. B 66 (2002), 245205.

[16] H.Z. Zhang, F. Huang, B. Gilbert, and J.F. Banfield, *Molecular dynamics simulations, thermodynamic analysis, and experimental study of phase stability of zinc sulfide nanoparticles*, J. Phys. Chem. B 107 (2003), pp. 13051–13060.

[17] H. Zhang, B. Gilbert, F. Huang, and J.F. Banfield, *Water-driven structure transformation in nanoparticles at room temperature*, Nature 424 (2003), pp. 1025–1029.

[18] Z.W. Wang, L.L. Daemen, Y.S. Zhao, C.S. Zha, R.T. Downs, X.D. Wang, Z.L. Wang, and R.J. Hemley, *Morphology-tuned wurtzite-type ZnS nanobelts*, Nat. Mater. 4 (2005), pp. 922–927.

[19] X.S. Fang, Y. Bando, G.Z. Shen, C.H. Ye, U.K. Gautam, P.M.F.J. Costa, C.Y. Zhi, C.C. Tang, and D. Golberg, *Ultrafine ZnS nanobelts as field emitters*, Adv. Mater. 19 (2007), pp. 2593–2596.

[20] X. Fang, Y. Bando, U.K. Gautam, C. Ye, and D. Golberg, *Inorganic semiconductor nanostructures and their field-emission applications*, J. Mater. Chem. 18 (2008), pp. 509–522.

[21] Z. Lin, B. Gilbert, Q.L. Liu, G.Q. Ren, and F. Huang, *A thermodynamically stable nanophase material*, J. Am. Chem. Soc. 128 (2006), pp. 6126–6131.

[22] W.T. Yao, S.H. Yu, L. Pan, L. Jing, Q.S. Wu, L. Zhang, and J. Jiang, *Flexible wurtzite-type ZnS nanobelts with quantum-size effects: a diethylenetriamine-assisted solvothermal approach*, Small 1 (2005), pp. 320–325.

[23] X. Fang, U.K. Gautam, Y. Bando, B. Dierre, T. Sekiguchi, and D. Golberg, *Multiangular branched ZnS nanostructures with needle-shaped tips: potential luminescent and field-emitter nanomaterial*, J. Phys. Chem. C 112 (2008), pp. 4735–4742.

[24] S.K. Panda, A. Datta, and S. Chaudhuri, *Nearly monodispersed ZnS nanospheres: synthesis and optical properties*, Chem. Phys. Lett. 440 (2007), pp. 235–238.

[25] L.W. Yin, Y. Bando, J.H. Zhan, M.S. Li, and D. Golberg, *Self-assembled highly faceted wurtzite-type ZnS single-crystalline nanotubes with hexagonal cross-sections*, Adv. Mater. 17 (2005), pp. 1972–1977.

[26] D. Moore, Y. Ding, and Z.L. Wang, *Hierarchical structured nanohelices of ZnS*, Angew. Chem., Int. Ed. 45 (2006), pp. 5150–5154.

[27] Z.W. Shan, G. Adesso, A. Cabot, M.P. Sherburne, S.A. Syed Asif, O.L. Warren, D.C. Chrzan, A.M. Minor, and A.P. Alivisatos, *Ultrahigh stress and strain in hierarchically structured hollow nanoparticles*, Nat. Mater. 7 (2008), pp. 947–952.

[28] B. Gilbert, F. Huang, H. Zhang, G.A. Waychunas, and J.F. Banfield, *Nanoparticles: strained and stiff*, Science 305 (2004), pp. 651–654.

[29] K.W. Urban, *Studying atomic structures by aberration-corrected transmission electron microscopy*, Science 321 (2008), pp. 506–510.

[30] S.J.L. Billinge and I. Levin, *The problem with determining atomic structure at the nanoscale*, Science 316 (2007), pp. 561–565.

[31] G. Ferey, C. Mellot-Draznieks, C. Serre, F. Millange, J. Dutour, S. Surble, and I. Margiolaki, *A chromium terephthalate-based solid with unusually large pore volumes and surface area*, Science 309 (2005), pp. 2040–2042.

[32] G. Férey, C. Serre, C. Mellot-Draznieks, F. Millange, S. Surblé, J. Dutour, and I. Margiolaki, *A hybrid solid with giant pores prepared by a combination of targeted chemistry, simulation, and powder diffraction*, Angew. Chem., Int. Ed. 43 (2004), pp. 6296–6301.

[33] C. Mellot-Draznieks, *Role of computer simulations in structure prediction and structure determination: from molecular compounds to hybrid frameworks*, J. Mater. Chem. 17 (2007), pp. 4348–4358.

[34] P.E. Lippens and M. Lannoo, *Calculation of the band gap for small CdS and ZnS crystallites*, Phys. Rev. B 39 (1989), p. 10935.

[35] K. Tóth, T.A. Pakkanen, P. Hirva, and J. Muilu, *Model calculations for surfaces and chemisorption processes of zinc-chalcogenide thin films by an* ab initio *cluster approach*, Surf. Sci. 277 (1992), pp. 395–406.

[36] J. Muilu and T.A. Pakkanen, Ab initio *study of small zinc sulfide crystallites*, Surf. Sci. 364 (1996), pp. 439–452.

[37] R.F. Curl and R.E. Smalley, *Probing C_{60}*, Science 242 (1988), pp. 1017–1022.

[38] B.C. Guo, S. Wei, J. Purnell, S. Buzza, and A.W. Castleman, Jr, *Metallo-carbohedrenes [$M_8C_{12}^+$ (M = V, Zr, Hf, and Ti)]: a class of stable molecular cluster ions*, Science 256 (1992), pp. 515–516.

[39] B.C. Guo, K.P. Kerns, and A.W. Castleman, Jr, *$Ti_8C_{12}^+$ metallo-carbohedrenes: a new class of molecular clusters?* Science 255 (1992), pp. 1411–1413.

[40] L. Lou, T. Guo, P. Nordlander, and R.E. Smalley, *Electronic structure of the hollow-cage M_8X_{12} clusters*, J. Chem. Phys. 99 (1993), pp. 5301–5305.

[41] E.C. Behrman, R.K. Foehrweiser, J.R. Myers, B.R. French, and M.E. Zandler, *Possibility of stable spheroid molecules of ZnO*, Phys. Rev. A 49 (1994), pp. R1543–R1548.

[42] A.A. Al-Sunaidi, A.A. Sokol, C.R.A. Catlow, and S.M. Woodley, *Structures of zinc oxide nanoclusters: as found by revolutionary algorithm techniques*, J. Phys. Chem. C 112 (2008), pp. 18860–18875.

[43] S. Hamad, C.R.A. Catlow, E. Spano, J.M. Matxain, and J.M. Ugalde, *Structure and properties of ZnS nanoclusters*, J. Phys. Chem. B 109 (2005), pp. 2703–2709.

[44] C.R.A. Catlow, S.A. French, A.A. Sokol, A.A. Al-Sunaidi, and S.M. Woodley, *Zinc oxide: a case study in contemporary computational solid state chemistry*, J. Comput. Chem. 29 (2008), pp. 2234–2249.

[45] M.W. Zhao, Y.Y. Xia, Z.Y. Tan, X.D. Liu, and L.M. Mei, *Design and energetic characterization of ZnO clusters from first-principles calculations*, Phys. Lett. A 372 (2007), pp. 39–43.

[46] B.L. Wang, X.Q. Wang, G.B. Chen, S.G. Nagase, and J.J. Zhao, *Cage and tube structures of medium-sized zinc oxide clusters $(ZnO)_n$ (n = 24, 28, 36, and 48)*, J. Chem. Phys. (2008), 144710 (1–6).

[47] J. Carrasco, F. Illas, and S.T. Bromley, *Ultralow-density nanocage-based metal-oxide polymorphs*, Phys. Rev. Lett. (2007), 235502 (1–4).

[48] M. Srnec and R. Zahradnik, *Small group IIa–VIa clusters and related systems: a theoretical study of physical properties, reactivity, and electronic spectra*, Eur. J. Inorg. Chem. (2007), pp. 1529–1543.

[49] A. Wootton and P. Harrowell, *Inorganic nanotubes stabilized by ion size asymmetry: energy calculations for AgI clusters*, J. Phys. Chem. B 108 (2004), pp. 8412–8418.

[50] M.-L. Sun, Z. Slanina, and S.-L. Lee, *Square/hexagon route towards the boron–nitrogen clusters*, Chem. Phys. Lett. 233 (1995), pp. 279–283.

[51] D.L. Strout, *Structure and stability of boron nitrides: isomers of $B_{12}N_{12}$*, J. Phys. Chem. A 104 (2000), pp. 3364–3366.

[52] Q.-B. Yan, X.-L. Sheng, Q.-R. Zheng, L.-Z. Zhang, and G. Su, *Family of boron fullerenes: general constructing schemes, electron counting rule, and* ab initio *calculations*, Phys. Rev. B (Condens. Matter Mater. Phys.) 78 (2008), 20140 (1–4).

[53] J.S. Pilgrim and M.A. Duncan, *Metallo-carbohedrenes: chromium, iron, and molybdenum analogs*, J. Am. Chem. Soc. 115 (1993), pp. 6958–6961.

[54] V. Tozzini, F. Buda, and A. Fasolino, *Spontaneous formation and stability of small GaP fullerenes*, Phys. Rev. Lett. 85 (2000), pp. 4554–4557.

[55] D. Zhang and R.Q. Zhang, *Geometrical structures and electronic properties of AlN fullerenes: a comparative theoretical study of AlN fullerenes with BN and C fullerenes*, J. Mater. Chem. 15 (2005), pp. 3034–3038.

[56] V. Tozzini, F. Buda, and A. Fasolino, *Fullerene-like III–V clusters: a density functional theory prediction*, J. Phys. Chem. B 105 (2001), pp. 12477–12480.

[57] S.A. Shevlin, Z.X. Guo, H.J.J. van Dam, P. Sherwood, C.R.A. Catlow, A.A. Sokol, and S.M. Woodley, *Structure, optical properties and defects in nitride (III–V) nanoscale cage clusters*, Phys. Chem. Chem. Phys. 10 (2008), pp. 1944–1959.

[58] N. Herron, J.C. Calabrese, W.E. Farneth, and Y. Wang, *Crystal structure and optical properties of $Cd_{32}S_{14}(SC_6H_5)_3$-DMF_4, a cluster with a 15 Angstrom CdS core*, Science 259 (1993), pp. 1426–1428.

[59] J. Xie, *Toward a facile one-step construction of quantum dots containing Zn_8S cores*, lnorg. Chem. 47 (2008), pp. 5564–5566.

[60] V.N. Soloviev, A. Eichhofer, D. Fenske, and U. Banin, *Molecular limit of a bulk semiconductor: size dependence of the 'Band Gap' in CdSe cluster molecules*, J. Am. Chem. Soc. 122 (2000), pp. 2673–2674.

[61] R. Bertoncello, M. Bettinelli, M. Casarin, C. Maccato, L. Pandolfo, and A. Vittadini, *An experimental and theoretical study of the electronic structure of zinc thiophenolate-capped clusters*, Inorg. Chem. 36 (1997), pp. 4707–4716.

[62] H.Z. Zhang, B. Gilbert, F. Huang, and J.F. Banfield, *Water-driven structure transformation in nanoparticles at room temperature*, Nature 424 (2003), pp. 1025–1029.

[63] B. Gilbert, F. Huang, Z. Lin, C. Goodell, H.Z. Zhang, and J.F. Banfield, *Surface chemistry controls crystallinity of ZnS nanoparticles*, Nano Lett. 6 (2006), pp. 605–610.

[64] B. Gilbert, H.Z. Zhang, F. Huang, J.F. Banfield, Y. Ren, D. Haskel, J.C. Lang, G. Srajer, A. Jurgensen, and G.A. Waychunas, *Analysis and simulation of the structure of nanoparticles that undergo a surface-driven structural transformation*, J. Chem. Phys. 120 (2004), pp. 11785–11795.

[65] N.S. Pesika, Z. Hu, K.J. Stebe, and P.C. Searson, *Quenching of growth of ZnO nanoparticles by adsorption of octanethiol*, J. Phys. Chem. B 106 (2002), pp. 6985–6990.

[66] B. Goswami, S. Pal, and P. Sarkar, *Theoretical studies of the effect of surface passivation on structural, electronic, and optical properties of zinc selenide clusters*, Phys. Rev. B (Condens. Matter Mater. Phys.) 76 (2007), 045323 (1–7).

[67] Z. Tang, Z. Zhang, Y. Wang, S.C. Glotzer, and N.A. Kotov, *Self-assembly of CdTe nanocrystals into free-floating sheets*, Science 314 (2006), pp. 274–278.

[68] B.L.T. Lau and H. Hsu-Kim, *Precipitation and growth of zinc sulfide nanoparticles in the presence of thiol-containing natural organic ligands*, Environ. Sci. Technol. 42 (2008), pp. 7236–7241.

[69] B. Gilbert and J.F. Banfield, *Molecular-scale processes involving nanoparticulate minerals in biogeochemical systems*, Rev. Mineral. Geochem. 59 (2005), pp. 109–155.

[70] B.R. Tagirov, O.M. Suleimenov, and T.M. Seward, *Zinc complexation in aqueous sulfide solutions: determination of the stoichiometry and stability of complexes via ZnS(cr) solubility measurements at 100°C and 150 bars*, Geochim. Cosmochim. Acta 71 (2007), pp. 4942–4953.

[71] G.W. Luther, S.M. Theberge, and D.T. Rickard, *Evidence for aqueous clusters as intermediates during zinc sulfide formation*, Geochim. Cosmochim. Acta 63 (1999), pp. 3139–3169.

[72] G.W. Luther and D.T. Rickard, *Metal sulfide cluster complexes and their biogeochemical importance in the environment*, J. Nanoparticle Res. 7 (2005), pp. 389–407.

[73] M.F. Hochella, Jr, S.K. Lower, P.A. Maurice, R.L. Penn, N. Sahai, D.L. Sparks, and B.S. Twining, *Nanominerals, mineral nanoparticles, and earth systems*, Science 319 (2008), pp. 1631–1635.

[74] M. Tiemann, F. Marlow, F. Brieler, and M. Linden, *Early stages of ZnS growth studied by stopped-flow UV absorption spectroscopy: effects of educt concentrations on the nanoparticle formation*, J. Phys. Chem. B 110 (2006), pp. 23142–23147.

[75] M. Tiemann, F. Marlow, J. Hartikainen, O. Weiss, and M. Linden, *Ripening effects in ZnS nanoparticle growth*, J. Phys. Chem. C 112 (2008), pp. 1463–1467.

[76] D. Erdemir, S. Chattopadhyay, L. Guo, J. Ilavsky, H. Amenitsch, C.U. Segre, and A.S. Myerson, *Relationship between self-association of glycine molecules in supersaturated solutions and solid state outcome*, Phys. Rev. Lett. 99 (2007), 115702 (1–4).

[77] S. Hamad, C.E. Hughes, C.R.A. Catlow, and K.D.M. Harris, *Clustering of glycine molecules in aqueous solution studied by molecular dynamics simulation*, J. Phys. Chem. B 112 (2008), pp. 7280–7288.

[78] J. Huang, T.C. Stringfellow, and L. Yu, *Glycine exists mainly as monomers, not dimers, in supersaturated aqueous solutions: Implications for understanding its crystallization and polymorphism*, J. Am. Chem. Soc. 130 (2008), pp. 13973–13980.

[79] S. Hamad, S. Cristol, and C.R.A. Catlow, *Simulation of the embryonic stage of ZnS formation from aqueous solution*, J. Am. Chem. Soc. 127 (2005), pp. 2580–2590.

[80] G.R. Helz, J.M. Charnock, D.J. Vaughan, and C.D. Garner, *Multinuclearity of aqueous copper and zinc bisulfide complexes: an EXAFS investigation*, Geochim. Cosmochim. Acta 57 (1993), pp. 15–25.

[81] H.Z. Zhang, J.R. Rustad, and J.F. Banfield, *Interaction between water molecules and zinc sulfide nanoparticles studied by temperature-programmed desorption and molecular dynamics simulations*, J. Phys. Chem. A 111 (2007), pp. 5008–5014.

[82] T. Huang, K. Tan, and M. Lin, *A theoretical exploration of the interaction of adsorptive molecules with the ZnS clusters*, J. Mol. Struct. THEOCHEM 821 (2007), pp. 101–105.

[83] Y. Sharifi and L.E. Achenie, *Using density functional theory to postulate a mechanism for zinc sulfide formation in a CVD reactor*, J. Cryst. Growth 307 (2007), pp. 440–447.

[84] J.M. Matxain, J.E. Fowler, and J.M. Ugalde, *Small clusters of II–VI materials: Zn_iS_i*, i = *1–9*, Phys. Rev. A 61 (2000), 053201 (1–8).

[85] A.D. Becke, *Density-functional thermochemistry. III. The role of exact exchange*, J. Chem. Phys. 98 (1993), pp. 5648–5652.

[86] W. Stevens, M. Krauss, H. Basch, and P.G. Jasien, *Relativistic compact effective potentials and efficient, shared-exponent basis-sets for the 3rd-row, 4th-row, and 5th-row atoms*, Can. J. Chem.-Revue Canadienne de Chimie 70 (1992), pp. 612–630.

[87] J.M. Matxain, A. Irigoras, J.E. Fowler, and J.M. Ugalde, *Electronic excitation energies of small Zn_iS_i clusters*, Phys. Rev. A 63 (2000), 013202 (1–7).

[88] C. Adamo and V. Barone, *Toward reliable adiabatic connection models free from adjustable parameters*, Chem. Phys. Lett. 274 (1997), pp. 242–250.

[89] J.M. Matxain, A. Irigoras, J.E. Fowler, and J.M. Ugalde, *Electronic excitation energies of Zn_iS_i clusters*, Phys. Rev. A 64 (2001), 013201 (1–7).

[90] J.M. Matxain, L.A. Eriksson, E. Formoso, M. Piris, and J.M. Ugalde, *Endohedral $(X@Zn_iS_i)^{(0,+/-)}$ $(i = 4–16)$ nanoclusters, X = Li, Na, K, Cl, Br*, J. Phys. Chem. C 111 (2007), pp. 3560–3565.

[91] H. Liu, S. Wang, G. Zhou, J. Wu, and W. Duana, *Structural, electronic, and magnetic properties of manganese-doped $Zn_{12}O_{12}$ clusters: a first-principles study*, J. Chem. Phys. 124 (2006), 174705.

[92] K. Chuchev and J.J. Belbruno, *Small, nonstoichiometric zinc sulfide clusters*, J. Phys. Chem. A 109 (2005), pp. 1564–1569.

[93] A. Burnin and J.J. Belbruno, *$Zn_nS_m^+$ cluster production by laser ablation*, Chem. Phys. Lett. 362 (2002), pp. 341–348.

[94] C. Roberts and R.L. Johnston, *Investigation of the structures of MgO clusters using a genetic algorithm*, Phys. Chem. Chem. Phys. 3 (2001), pp. 5024–5034.

[95] A. Kasuya, R. Sivamohan, Y.A. Barnakov, I.M. Dmitruk, T. Nirasawa, V.R. Romanyuk, V. Kumar, S.V. Mamykin, K. Tohji, B. Jeyadevan, K. Shinoda, T. Kudo, O. Terasaki, Z. Liu, R.V. Belosludov, V. Sundarajan, Y. Kawazoe, *Ultra-stable nanoparticles of CdSe revealed from mass spectrometry*, Nat. Mater. 3 (2004), pp. 99–102.

[96] S.M. Woodley, A.A. Sokol, and C.R.A. Catlow, *Structure prediction of inorganic nanoparticles with predefined architecture using a genetic algorithm*, Zeitschrift Fur Anorganische Und Allgemeine Chemie 630 (2004), pp. 2343–2353.

[97] A. Burnin, E. Sanville, and J.J. BelBruno, *Experimental and computational study of the Zn_nS_n and $Zn_nS_n^+$ clusters*, J. Phys. Chem. A 109 (2005), pp. 5026–5034.

[98] E. Sanville, A. Burnin, and J.J. BelBruno, *Experimental and computational study of small $(n = 1–16)$ stoichiometric zinc and cadmium chalcogenide clusters*, J. Phys. Chem. A 110 (2006), pp. 2378–2386.

[99] S.M. Woodley and R. Catlow, *Crystal structure prediction from first principles*, Nat. Mater. 7 (2008), pp. 937–946.

[100] E. Spano, S. Hamad, and C.R.A. Catlow, *Computational evidence of bubble ZnS clusters*, J. Phys. Chem. B 107 (2003), pp. 10337–10340.

[101] S. Hamad, S. Cristol, and C.R.A. Catlow, *Surface structures and crystal morphology of ZnS: computational study*, J. Phys. Chem. B 106 (2002), pp. 11002–11008.

[102] H.W. Kroto, *The stability of the fullerenes Cn, with n = 24, 28, 32, 36, 50, 60 and 70*, Nature 329 (1987), pp. 529–531.

[103] J.M. Matxain, L.A. Eriksson, J.M. Mercero, J.M. Ugalde, E. Spano, S. Hamad, and C.R.A. Catlow, *Electronic excitation energies of Zn_iS_i nanoparticles*, Nanotechnology 17 (2006), pp. 4100–4105.

[104] P. Calandra, A. Longo, and V. Turco Liveri, *Synthesis of ultra-small ZnS nanoparticles by solid–solid reaction in the confined space of AOT reversed micelles*, J. Phys. Chem. B 107 (2003), pp. 25–30.

[105] R. Rossetti, R. Hull, J.M. Gibson, and L.E. Brus, *Excited electronic states and optical spectra of ZnS and CdS crystallites in the ~15 to 50 Å size range: evolution from molecular to bulk semiconducting properties*, J. Chem. Phys. 82 (1985), pp. 552–559.

[106] E. Spano, S. Hamad, and C.R.A. Catlow, *ZnS bubble clusters with onion-like structures*, Chem. Commun. (2004), pp. 864–865.

[107] S. Hamad and C.R.A. Catlow, *Computational study of the relative stabilities of ZnS clusters, for sizes between 1 and 4 nm*, J. Cryst. Growth 294 (2006), pp. 2–8.

[108] S. Pal, B. Goswami, and P. Sarkar, *Size-dependent properties of Zn_mS_n clusters: a density-functional tight-binding study*, J. Chem. Phys. 123 (2005), 044311 (1–9).

[109] S. Pal, B. Goswami, and P. Sarkar, *Size-dependent properties of hollow ZnS nanoclusters*, J. Phys. Chem. C 112 (2008), pp. 6307–6312.

[110] Y. Yin, R.M. Rioux, C.K. Erdonmez, S. Hughes, G.A. Somorjai, and A.P. Alivisatos, *Formation of hollow nanocrystals through the nanoscale kirkendall effect*, Science 304 (2004), pp. 711–714.

[111] S. Pal, B. Goswami, and P. Sarkar, *Controlling the shape of nanocrystals*, J. Phys. Chem. C 111 (2007), pp. 16071–16075.

[112] B.J. Morgan and P.A. Madden, *Pressure-driven sphalerite to rock salt transition in ionic nanocrystals: a simulation study*, Nano Lett. 4 (2004), pp. 1581–1585.

[113] B.J. Morgan and P.A. Madden, *A molecular dynamics study of structural relaxation in tetrahedrally coordinated nanocrystals*, Phys. Chem. Chem. Phys. 9 (2007), pp. 2355–2361.

[114] B.J. Morgan and P.A. Madden, *Pressure-driven phase transitions in crystalline nanoparticles: surface effects on hysteresis*, J. Phys. Chem. C 111 (2007), pp. 6724–6731.

[115] B.J. Morgan, *Molecular dynamics simulation of the six- to four-coordinate pressure-driven transition in MX nanocrystals: mechanistic consequences of Σ_3 grain boundaries in the high-pressure starting structure*, Phys. Rev. B 78 (2008), 024110 (1–10).

[116] K. Doll, J.C. Schon, and M. Jansen, *Structure prediction based on* ab initio *simulated annealing for boron nitride*, Phys. Rev. B (Condens. Matter Mater. Phys.) 78 (2008), 144110 (1–10).

[117] K. Doll, J.C. Schon, and M. Jansen, *Global exploration of the energy landscape of solids on the* ab initio *level*, Phys. Chem. Chem. Phys. 9 (2007), pp. 6128–6133.

[118] E.V. Shevchenko, D.V. Talapin, N.A. Kotov, S. O'Brien, and C.B. Murray, *Structural diversity in binary nanoparticle superlattices*, Nature 439 (2006), pp. 55–59.

[119] D.C. Sayle, S. Seal, Z. Wang, B.C. Mangili, D.W. Price, A.S. Karakoti, S. Kuchibhatla, Q. Hao, G. Mobus, X. Xu, et al., *Mapping nanostructure: a systematic enumeration of nanomaterials by assembling nanobuilding blocks at crystallographic positions*, ACS Nano 2 (2008), pp. 1237–1251.

[120] D.C. Sayle, B.C. Mangili, J. Klinowski, and T.X.T. Sayle, *Simulating self-assembly of ZnS nanoparticles into mesoporous materials*, J. Am. Chem. Soc. 128 (2006), pp. 15283–15291.

[121] K. Wright and J.D. Gale, *Interatomic potentials for the simulation of the zinc-blende and wurtzite forms of ZnS and CdS: bulk structure, properties, and phase stability*, Phys. Rev. B (2004), 032511 (1–8).

[122] H.Z. Zhang, B. Chen, B. Gilbert, and J.F. Banfield, *Kinetically controlled formation of a novel nanoparticulate ZnS with mixed cubic and hexagonal stacking*, J. Mater. Chem. 16 (2006), pp. 249–254.

[123] Y.-C. Zhu, Y. Bando, and Y. Uemura, *ZnS-Zn nanocables and ZnS nanotubes*, Chem. Commun. 7 (2003), pp. 836–837.

[124] H. Shao, X. Qian, and B. Huang, *Fabrication of single-crystal ZnO nanorods and ZnS nanotubes through a simple ultrasonic chemical solution method*, Mater. Lett. 61 (2007), pp. 3639–3643.

[125] H. Zhang, S. Zhang, S. Pan, G. Li, and J. Hou, *A simple solution route to ZnS nanotubes and hollow nanospheres and their optical properties*, Nanotechnology 15 (2004), pp. 945–948.

[126] J. Hu, Y. Bando, J. Zhan, and D. Golberg, *Sn-filled single-crystalline wurtzite-type ZnS nanotubes*, Angew. Chem., Int. Ed. 43 (2004), pp. 4606–4609.

[127] Z. Wang, X.-F. Qian, Y. Li, J. Yin, and Z.-K. Zhu, *Large-scale synthesis of tube-like ZnS and cable-like ZnS–ZnO arrays: preparation through the sulfuration conversion from ZnO arrays via a simple chemical solution route*, J. Solid State Chem. 178 (2005), pp. 1589–1594.

[128] S. Pal, B. Goswami, and P. Sarkar, *Theoretical study on the structural, energetic, and optical properties of ZnS nanotube*, J. Phys. Chem. C 111 (2007), pp. 1556–1559.

[129] L. Li, M. Zhao, X. Zhang, Z. Zhu, F. Li, J. Li, C. Song, X. Liu, and Y. Xia, *Theoretical insight into faceted ZnS nanowires and nanotubes from interatomic potential and first-principles calculations*, J. Phys. Chem. C 112 (2008), pp. 3509–3514.

[130] X. Zhang, M. Zhao, S. Yan, T. He, W. Li, X. Lin, Z. Xi, Z. Wang, X. Liu, and Y. Xia, *First-principles study of ZnS nanostructures: nanotubes, nanowires and nanosheets*, Nanotechnology 19 (2008), 305708 (1–6).

[131] X. Zhang, M. Zhao, T. He, W. Li, X. Lin, Z. Wang, Z. Xi, X. Liu, and Y. Xia, *Theoretical models of ZnS nanoclusters and nanotubes: first-principles calculations*, Solid State Commun. 147 (2008), pp. 165–168.

[132] S. Pal, R. Sharma, B. Goswami, and P. Sarkar, *Theoretical prediction of ring structures for ZnS quantum dots*, Chem. Phys. Lett. 467 (2009), pp. 365–368.